OXFORD

G3 Genes | Genomes | Genetics

G3, 2021, 11(11), jkab303
DOI: 10.1093/g3journal/jkab303
Advance Access Publication Date: 26 August 2021
Investigation

Insm1, Neurod1, and Pax6 promote murine pancreatic endocrine cell development through overlapping yet distinct RNA transcription and splicing programs

Karrie D. Dudek,[1,2] Anna B. Osipovich,[2,3] Jean-Philippe Cartailler,[2] Guoquing Gu,[1,2] and Mark A., Magnuson[1,2,3,*]

[1]Department of Cell and Developmental Biology, Vanderbilt University, Nashville, TN 37232, USA
[2]Center for Stem Cell Biology, Vanderbilt University, Nashville, TN 37232, USA
[3]Department of Molecular Physiology and Biophysics, Vanderbilt University, Nashville, TN 37232, USA

*Corresponding author: Vanderbilt University, 9465 MRB-IV, 2213 Garland Avenue, Nashville, TN 37232-0494, USA. Email: mark.magnuson@vanderbilt.edu

Abstract

Insm1, *Neurod1*, and *Pax6* are essential for the formation and function of pancreatic endocrine cells. Here, we report comparative immunohistochemical, transcriptomic, functional enrichment, and RNA splicing analyses of these genes using gene knock-out mice. Quantitative immunohistochemical analysis confirmed that elimination of each of these three factors variably impairs the proliferation, survival, and differentiation of endocrine cells. Transcriptomic analysis revealed that each factor contributes uniquely to the transcriptome although their effects were overlapping. Functional enrichment analysis revealed that genes downregulated by the elimination of *Insm1*, *Neurod1*, and *Pax6* are commonly involved in mRNA metabolism, chromatin organization, secretion, and cell cycle regulation, and upregulated genes are associated with protein degradation, autophagy, and apoptotic process. Elimination of *Insm1*, *Neurod1*, and *Pax6* impaired expression of many RNA-binding proteins thereby altering RNA splicing events, including for *Syt14* and *Snap25*, two genes required for insulin secretion. All three factors are necessary for normal splicing of *Syt14*, and both *Insm1* and *Pax6* are necessary for the processing of *Snap25*. Collectively, these data provide new insights into how *Insm1*, *Neurod1*, and *Pax6* contribute to the formation of functional pancreatic endocrine cells.

Keywords: pancreas; endocrine progenitor cells; gene expression; alternative RNA splicing

Introduction

During pancreas development, the formation of islets of Langerhans requires formation of an endocrine cell-specific gene regulatory network (GRN). Prior studies have identified multiple transcription factors (TFs) that contribute to endocrine cell development (Arda *et al.* 2013; Osipovich *et al.* 2021). Among these, Neurog3 plays an especially important role. By activating a downstream cascade of pro-endocrine TFs, Neurog3 initiates formation of the endocrine cell-specific GRN (Gu *et al.* 2002; Ejarque *et al.* 2013; Bechard *et al.* 2016). In its absence, the fate of pancreatic pre-endocrine cells is redirected toward the ductal lineage and no endocrine cells are formed (Gradwohl *et al.* 2000; Schwitzgebel *et al.* 2000; Wang *et al.* 2010; Osipovich *et al.* 2021). In contrast, when other pro-endocrine TFs downstream of Neurog3 are eliminated, including Insm1, Neurod1, and Pax6, pancreatic endocrine-like cells are formed that exhibit marked defects in proliferation and/or hormone expression, suggesting that each of these factors, in turn, regulates a subnetwork of genes (Naya *et al.* 1997; Sander *et al.* 1997; St-Onge *et al.* 1997; Huang *et al.* 2000; Heller *et al.* 2004; Gierl *et al.* 2006; Mellitzer *et al.* 2006; Osipovich *et al.* 2014).

TFs activate target genes by directly binding DNA in promoter regions, and ChIP-Seq has been widely used to identify genome-wide TF binding sites. Previous ChIP-Seq studies using cell lines have identified many binding sites for Insm1, Neurod1, and Pax6. Analysis of Insm1 and Neurod1 binding sites in a pancreatic β-cell line derived from adult islets has shown that Insm1, Neurod1, and Foxa2 frequently co-bind to the same genomic regions. However, these analyses have also revealed that only 32% of genes in adult β-cells that are regulated by *Insm1* have nearby Insm1 binding (Jia *et al.* 2015). Similarly, while both Pax6 and Neurod1 often bind to enhancers that are active in insulinoma cells, the binding of both factors occurs at only 40% of such binding sites (Lizio *et al.* 2015). Furthermore, while there is a large degree of overlap in the binding of Neurod1 and Pax6, Pax6 exhibits both activating and repressive functions in mouse and human β-cell lines (Swisa *et al.* 2017).

RNA processing is also a vitally important process that is regulated during development. There are hundreds of different RNA-binding proteins (RBPs) that affect polyadenylation, stabilization, and localization dynamics of mRNA. Some of these proteins also introduce nucleotide modifications and cause differential

Received: May 05, 2021. **Accepted:** August 19, 2021
© The Author(s) 2021. Published by Oxford University Press on behalf of Genetics Society of America.
This is an Open Access article distributed under the terms of the Creative Commons Attribution-NonCommercial-NoDerivs licence (http://creativecommons.org/licenses/by-nc-nd/4.0/), which permits non-commercial reproduction and distribution of the work, in any medium, provided the original work is not altered or transformed in any way, and that the work is properly cited. For commercial re-use, please contact journals.permissions@oup.com

splicing of introns and exons (Licatalosi and Darnell 2010; Wickramasinghe and Venkitaraman 2016; Manning and Cooper 2017; Carazo *et al.* 2019). Alternative RNA splicing significantly enhances transcriptome diversity, and it is important for cell differentiation (Fiszbein and Kornblihtt 2017). Indeed, Singer *et al.* (2019) have recently reported that the alternative splicing of *Pax6*, which requires recruitment of RBPs by the lncRNA *Pauper*, alters both its transcriptional activity and DNA binding specificity. It has also recently been shown in islets from individuals with type 2 diabetes that many RBPs are dysregulated and that this may impair correct RNA splicing (Jeffery *et al.* 2019).

In this study, we performed immunohistochemical and bulk transcriptomic analyses to directly compare the effects of eliminating *Insm1*, *Neurod1*, and *Pax6* during endocrine cell development. Our findings indicate that these three TFs individually and coordinately regulate the expression of common and unique sets of genes necessary for the proliferation and function of pancreatic endocrine cells. Additionally, we find that Insm1, Neurod1, and Pax6 differentially affect the splicing of genes, thereby adding complexity to pancreatic endocrine cell proteomes.

Materials and methods

Mice and genotyping

Insm1$^{tm1.1Mgn}$ (*Insm1*^{GFPCre}) (Osipovich *et al.* 2014) and *Neurod1*^{tm1Jle} (*Neurod1*^{LacZ}) (Miyata *et al.* 1999) mice were maintained in a CD-1 background. *Pax6*^{tm2Pgr} (*Pax6*^{flox}) mice were obtained from Jackson Laboratory and kept in a C57Bl6/J background (Ashery-Padan *et al.* 2000; Sun *et al.* 2008). All animal experimentation was performed under the Vanderbilt University Institutional Animal Care and Use Committee's oversight. The *Insm1*^{GFPCre} allele expresses a GFP-Cre fusion protein that contains a nuclear localization sequence and were genotyped as previously described (Osipovich *et al.* 2014). *Pax6*^{flox} mice contain loxP sites flanking the initiation codon in exon 4 and exon 6 (the paired domain), requiring Cre activity for excision and were genotyped using the primer pairs 5′-CCTAACAGAGCCCCGTATTC (forward) and 5′-GCCCAACAGTCCAGAGAAAG (reverse). In Neurod1LacZ mice, Neurod1 coding sequences were replaced with a LacZ reporter (Miyata et al. 1999) and therefore intrinsically lack Neurod1 expression. To detect wild-type Neurod1 and Neurod1LacZ we used either 5′-ACCATGCACTCTGTACGCATT (forward) or 5′-GAGAACTGAGACACTCATCTG (forward) in combination with 5′-AAACGCCGAGTTAAAGCCATC (reverse), respectively.

Timed matings and tissue collection

Embryos were isolated from timed matings where noon of the day that vaginal plugs were observed was designated E0.5. Embryonic day (E) 15.5 animals were dissected into ice-cold PBS and visually genotyped for the presence of *Insm*^{GFPCre} allele based on green fluorescence. For PCR genotyping, embryonic tissues were digested at 55°C in 100 µl of PCR lysis buffer (1× PCR buffer, 0.1% Triton X-100, 100 µg/ml Proteinase K), inactivated at 90°C for 15 min and used for PCR. Whole pancreas was dissected and either processed for fluorescence-activated cell sorting (FACS) or frozen in OCT for immunostaining analyses.

Immunofluorescence

Pancreata were routinely fixed in 2% paraformaldehyde for 2 h at room temperature, incubated in 30% sucrose in PBS overnight on a shaker, then mounted using Tissue Tek O.C.T. compound and stored at −80°C. Immunofluorescence staining of frozen tissue sections was performed as previously described (Burlison *et al.* 2008). Ten µm tissue sections were stained using anti-GFP (1:500, ThermoFisher, #A10262), insulin (1:1000, Invitrogen, #PA1-26938), glucagon (1:100, Milipore, #AB932), somatostatin (1:1000, Linco), pancreatic polypeptide (1:1000, Linco), and/or Ki67 (1:500, ThermoFisher, #RM-9106-S1) antibodies, and ProLong Gold antifade reagent with DAPI (Life Technologies, #P36941) used to mount coverslips. TUNEL (TMR red) assays were performed following the manufacturer's protocol (ROCHE). Respective images were obtained via confocal microscopy using an LSM 510 Meta microscope at 20× magnification. The image processing software, ImageJ (National Institute of Health), was used to manually identify and quantify fluorescently-positive cells (Schneider *et al.* 2012). The percentage of GFP-positive cells expressing islet hormones were calculated. Three different biological replicates from each genotype and at least 500 cells were analyzed for each measurement.

Fluorescence-activated cell sorting

Pancreatic cells were dispersed into a single-cell suspension by incubation for 5 min at 37°C in Accumax (Sigma) containing 50 µg/ml DNase I. Reactions were quenched by the addition of sorting buffer [FACS staining buffer (R&D Systems), DNAse (1:1000)]. Cells were then filtered through a 35 µm nylon mesh into a FACS tube (Corning), washed once with FACS staining buffer, centrifuged at 1100 rpm for 3 min, then re-suspended in 500 µl of FACS sorting buffer (Osipovich *et al.* 2014). 7-aminoactinomycin (7-AAD) was added at a concentration of 1:1000 immediately before sorting using either a Benton Dickenson FACS Aria-II or Aria-III instrument to distinguish between live and dead cells. GFP-positive, 7-AAD negative cells were collected directly into Trizol LS (Invitrogen) containing 40 µg/ml of mussel glycogen (Roche/Sigma). An average of 6000 cells was obtained per embryo sample.

RNA isolation, library construction, and RNA-Seq

Three replicate samples for each genotype were collected, and total RNA was isolated using Trizol LS then treated with DNase I (Life Technologies). RNA was column-purified using the RNA Clean and Concentrator Kit (Zymo Research) and previously published protocols (Choi *et al.* 2012). RNA integrity was determined using an Agilent 2100 Bioanalyzer (Agilent Technologies, CA, USA), and samples with an RNA integrity number (RIN) of 7.0 or greater were used for RNA-Seq. All samples were amplified using the SMART-Seq Ultra Low Input RNA Kit (TAKARA/Clontech) at 10 cycles, except for the *Neurog3*$^{GFP/+}$ and *Neurog3*$^{GFP/GFP}$ samples, which were prepared using the Ovation RNA-Seq System V2 (NuGEN). cDNA was prepared using the Low Input Library Kit (Clontech) and sequenced using either an Illumina HiSeq3000 genome analyzer to obtain paired-end, 75-bp reads, or Illumina NovaSeq6000 to get paired-end, 100-bp reads. RNA samples were sequenced to an average depth of ~5.0×10^7 reads. RNA-Seq data have been deposited in ArrayExpress (accession no. E-MTAB-10262).

Bioinformatic analysis of RNA-Seq

FastQ files were routinely processed then sanitized using FastQC (https://www.bioinformatics.babraham.ac.uk/projects/fastqc/) (last accessed 2021-08-31) and TrimGalore (https://www.bioinformatics.babraham.ac.uk/projects/trim_galore/) (last accessed 2021-08-31), respectively. Individual reads were aligned to the mouse genome (mm-10) using Spliced Transcripts Alignment to a Reference (STAR) software (Dobin *et al.* 2013). Pairwise differential gene expression analyses were performed using HTSeq (Anders

et al. 2015) to obtain read counts, and DESeq2 was used (Love *et al.* 2014) to quantify and display the differences. Only genes that exceeded an adjusted *P*-value ≤0.05 were included in the analysis. Gene ontology (GO) analyses were performed using the online Database for Annotation, Visualization, and Integrated Discovery (DAVID v6.8) (Huang da *et al.* 2009a,b). *Neurog3*$^{GFP/+}$ and *Neurog3*$^{GFP/GFP}$ samples were separately analyzed as described (Osipovich *et al.* 2021).

Bioinformatic analysis of ChIP-Seq

ChIP-Seq datasets for INSM1 and NEUROD1 binding sites were obtained from ArrayExpress (E-GEOD-54046). Both datasets were obtained using an insulinoma cell line propagated from RIP1-Tag2 transgenic mice (Jia, *et al.* 2015). Snakemake (5.2.4), a workflow management system, was used to manage the data processing. FastQC (0.11.7) returned a quality score report on each sample's sequences before and after Trimgalore (0.6.5) discarded sequences with a read length shorter than 20 bp were discarded and trimmed read ends that do not meet the threshold of 20. Trimmed sequences were used by the RNA-Seq aligner Bowtie2 (2.3.5) to align against the mouse genome (gencode 17; GRCm38). On average, 95% of reads were mapped to the reference per sample. Samtools (1.9) converted the SAM files into BAM files and filtered out alignments with a lower MAPQ value than 10, and sort alignments by leftmost coordinates and by read name. Macs2 (2.2.6) was used to perform peak calling on the samples using default parameters for bandwidth and effective genome size. The resulting BED files were modified by bedtools (2.26.0) for pile-up visualization via IGV. Unmodified BED files were reported as very high-quality data by phantompeakqualtools (1.2.2).

Differential splice variant analysis

DSV analysis was performed using the previously described RNA-Seq datasets from control and knock-out (KO) embryos at E15.5. Snakemake (5.2.4), a workflow management system, was used to call five programs necessary to process the samples. FastQC (0.11.8) returned a quality score report on each sample's sequences before and after Trimgalore (0.5.0) trimmed the sequences. Trimmed paired-end sequences were passed to STAR (2.6.0), an RNA-seq aligner, to align against the mouse genome (gencode 17; GRCm38), and gene counts for each sample were returned. The average uniquely mapped reads count per sample was 52M (89%). QoRTs (Quality of RNA-Seq toolset) converts the gene counts format for analysis in JunctionSeq. Lastly, Multiqc (1.7) compiled the final summary output from the other jobs into a single report. Gene counts for each sample were passed to R (3.5.3) to do a quality control assessment before analysis. Quality control assessment included analyzing a box plot of normalized sample counts, principal component analysis (PCA) plot, sample to sample heatmap clustering, and a density plot of the normalized counts. All samples passed the quality control assessment. Each sample's QoRTS formatted gene counts were run through JunctionSeq (1.12.1) to determine any differential gene expression through alternative splicing between the KO and control groups.

Sashimi plots and exon junction visualization

Plots of read coverage across exons and corresponding sashimi plots were generated using the Integrative Genomics Viewer (IGV) platform (Robinson *et al.* 2011). Indexed BAM files from each KO dataset were uploaded directly to IGV for analysis, and mm10 was used as the reference genome. All tracks are set to the same read count scale for a given locus.

Results

An integrated analysis of *Insm1*, *Neurod1*, and *Pax6*, three *Neurog3*-dependent pro-endocrine TFs

Comparison of the gene expression profiles of purified *Neurog3*$^{GFP/+}$ and *Neurog3*$^{GFP/GFP}$ (*Neurog3* KO) cells from E15.5 embryos by bulk RNA-Seq (Osipovich *et al.* 2021) revealed a marked reduction in the expression of pro-endocrine TFs *Insm1*, *Neurod1*, and *Pax6* (Supplementary Figure S1A). The marked dysregulation of these genes provides further evidence that each lies downstream of *Neurog3* in a Neurog3-driven endocrine cell-specific gene regulatory network (Supplementary Figure S1B) essential for the formation and function of pancreatic endocrine cells (Naya *et al.* 1997; St-Onge *et al.* 1997; Gierl *et al.* 2006; Mellitzer *et al.* 2006).

To systematically assess and compare the independent effects of *Insm1*, *Neurod1*, and *Pax6* in developing endocrine cells, we intercrossed mice containing *Insm1*^{GFPCre}, *Neurod1*^{LacZ}, and *Pax6*^{flox} alleles. From timed matings, we obtained embryos that were heterozygous for *Insm1* (*Insm1*$^{+/-}$) for use as controls, embryos that were globally deficient in *Insm1* (*Insm1* KO) or *Neurod1* (*Neurod1* KO), and embryos that lacked *Pax6* specifically in *Insm1*-expressing cells (*Pax6* KO) (Figure 1). Our strategy took advantage of the expression profile of *Insm1*, specifically that it is expressed in developing endocrine cells, that it is maintained in all endocrine cell types through adulthood, and that it is absent in exocrine pancreas. Green fluorescence produced by the *Insm1*^{GFPCre} allele enabled us to purify endocrine cells by FACS from E15.5 embryos for RNA-Seq analysis and to accurately identify pancreatic endocrine cells by immunohistochemistry in tissue samples from E18.5 embryos (Figure 1). The findings were then comparatively analyzed.

Mice lacking Insm1, Neurod1, or Pax6 exhibit defects in endocrine cell differentiation, proliferation, and apoptosis

Immunofluorescence staining and morphometric analysis of pancreatic tissues from *Insm1*$^{+/-}$ (control) and *Insm1* KO, *Neurod1* KO, and *Pax6* KO embryos at E18.5 was done by co-staining and quantifying the percentage of pancreatic hormone-positive cells, cell proliferation marker Ki67-positive, or apoptotic TUNEL-positive cells per total number of GFP-positive endocrine cells.

Similar to prior reports, embryos that lack *Insm1* exhibit both a disruption in endocrine cell organization and a reduced number of endocrine cells (Gierl *et al.* 2006; Osipovich *et al.* 2014). *Insm1* KO pancreata were again seen to have a lower number of insulin-, glucagon-, and somatostatin-expressing endocrine cells, and an increase in pancreatic polypeptide-expressing cells, indicating profound defects in endocrine differentiation and lineage specification (Figure 2, B, F, and I–L). Immunostaining with Ki67 revealed reduced proliferation of the *Insm1* KO endocrine cells (3.6% vs. 15% of control cells) (Figure 3, B, F, I, and J), whereas the number of apoptotic cells between the control and KO cells was unchanged.

As in previous studies, *Neurod1* KO embryos also exhibited a lower overall number of endocrine cells, disrupted islet organization, and increased percentage of pancreatic polypeptide-expressing endocrine cells increased (Figure 2, C, G, and I–L). The *Neurod1* KO embryos had fewer Ki67-positive endocrine cells (2.8% vs. 15% in the controls) and a marked increase in TUNEL-positive cells (4.5% vs. 0.6% in control animals) (Figure 3, C, G, I, and J), which is also similar to prior reports (Naya *et al.* 1997; Romer *et al.* 2019).

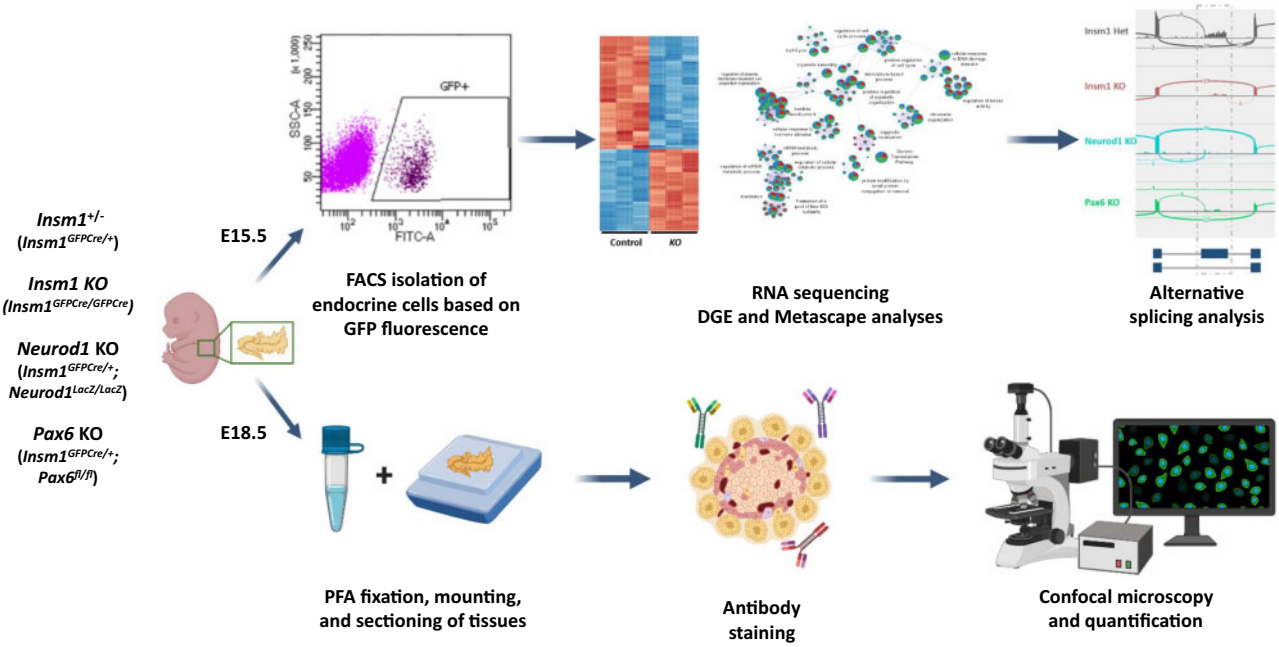

Figure 1 An integrated approach for analyzing the roles of *Insm1*, *Neurod1*, and *Pax6 in* pancreatic endocrine cell development. Control and KO embryos were collected at either E15.5 or E18.5. GFP-positive cells from E15.5 pancreata were FACS sorted and collected for RNA-Seq, followed by differential expression, Metascape, and differential splicing analyses. Pancreata from E18.5 embryos were fixed in PFA, sections stained for nuclear GFP signal, endocrine hormones, Ki67 and TUNEL reporter, and marked cells were subsequently quantified. Schematic was created with BioRender.com.

Similarly, analysis of the *Pax6* KO embryos revealed disorganized endocrine islets and a reduced overall number of endocrine cells. However, in these mice, there was a marked decrease in the number of glucagon-positive cells (Figure 2, D and J), although the numbers of other hormone-expressing GFP-positive cells were not significantly affected (Figure 2, H, K, and L). There was also a considerable reduction in the number of Ki67-positive cells in the *Pax6* KO animals (4% vs. 15% in the controls) (Figure 3, D and I) and an increase in the number of TUNEL-positive endocrine cells (Figure 3, H and J). Notably, we had difficulty obtaining *Insm1*$^{GFPCre/+}$, *Pax6* KO embryos at E18.5, and only succeeded in obtaining two embryos of the sought-after genotype out of 62 embryos genotyped ($P = 4.77E^{-05}$ by chi-squared test), indicating that the haploinsufficiency of *Insm1* in the setting of a *Pax6* KO impairs embryonic survival compared to the effects of a *Pax6* KO alone (Figure 3K).

Together, these analyses indicate that mice lacking *Insm1*, *Neurod1*, or *Pax6* have abnormal islet morphologies, a reduced number of endocrine cells, and varying defects in differentiation toward hormone-expressing cells. Moreover, all three KOs exhibited decreased endocrine cell proliferation rates, with both the *Neurod1* and *Pax6* KOs also showing increased apoptosis.

Pancreatic pre-endocrine cells lacking *Insm1*, *Neurod1*, and *Pax6* have distinct transcriptional profiles

Next, to better understand how each factor contributes to the pro-endocrine cell transcriptome, we performed bulk RNA-Seq on FACS-purified cell populations isolated from E15.5 embryos. Cells were isolated at this earlier time point to minimize variance in gene expression caused by maturation toward specific endocrine subtypes. Hierarchical clustering and PCA of the 12 RNA-Seq samples revealed tight clustering by genotype, indicating the low variance between samples and that each condition analyzed has a unique transcriptional profile (Supplementary Figure S2, A and B).

Dysregulated expression of genes involved in hormone secretion, RNA metabolism and processing, and cell development in *Insm1* KO endocrine cells

We previously reported the gene expression profile of both *Insm1*$^{+/-}$ and *Insm1* KO mice at E15.5 using a legacy RNA amplification and sequencing method (Osipovich *et al.* 2014). To accurately compare the transcriptomes of the three TF KOs in this study, we collected new *Insm1* KO datasets using the methods, reagents, and instrumentation described herein. A comparison of the two different *Insm1*$^{+/-}$ and *Insm1* KO datasets indicated that they clustered first by amplification method (Nugen vs. Clontech) and secondarily by genotype (*Insm1*$^{+/-}$ control vs. *Insm1* KO), consistent with a method-dependent batch effect. However, a linear regression analysis of the $\log_2$-fold changes of differentially expressed genes from the old and new datasets showed strong correlation ($R^2 = 0.85$) (Supplementary Figure S3, A–C).

Analysis of the new *Insm1*$^{+/-}$ and *Insm1* KO datasets by DESeq revealed a total of 4,694 differentially expressed genes, 2,265 were categorized as downregulated genes (DRGs) and 2429 upregulated genes (URGs) in the KO compared to control embryos (*P*-value ≤ 0.05) (Supplementary Figures S2C, S4, A and B and Table S1). Among the top DRGs were numerous TFs known to control endocrine cell development, including both *Sox9* (McDonald *et al.* 2012) and *Mnx1*, which is necessary for endocrine cell fate allocation and in later stages for maintaining the β-cell fate (Sund *et al.* 2001; Wang *et al.* 2002; Pan *et al.* 2015). Also, among the DRGs were the TF *Bhlhe23*, the histone modifiers *Hist1h2bf* and *Histh2bb*, and genes involved in the trafficking and secretion of insulin (*Avp, Chgb*) (Supplementary Figure S4C). GO and pathway enrichment analysis results from DRGs revealed enrichment in genes involved in cell projection morphogenesis (*Bdnf*, *Brsk2*, *Camk2b*,

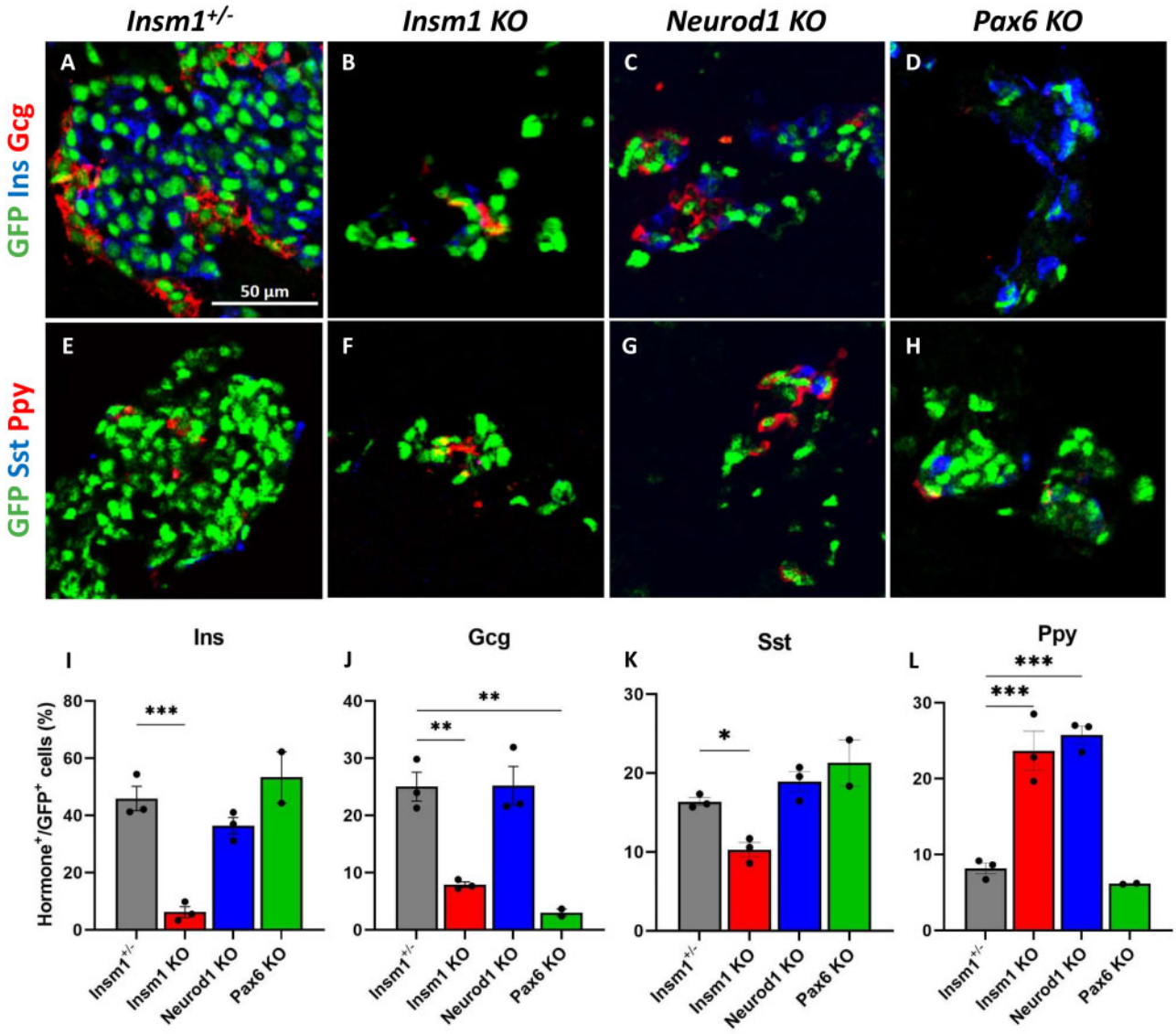

Figure 2 Impaired differentiation of pancreatic endocrine cells in *Insm1*, *Neurod1*, and *Pax6* KO embryos. (A–D) Immunofluorescence labeling of pancreata from E18.5 *Insm1*^{GFP}-expressing embryos using antibodies against GFP (green) that marks pre-endocrine cells, and pancreatic hormones insulin (Ins, blue), and glucagon (Gcg, red). Compared with *Insm1*$^{+/-}$ mice (A), mice lacking *Insm1* (B), *Neurod1* (C), and *Pax6* (D) exhibit a decrease in total number of endocrine cells, altered endocrine cell morphology and numbers of hormone expressing cells. (E–H) Immunofluorescence labeling of pancreata from E18.5 embryos using antibodies against GFP (green), pancreatic polypeptide (Ppy, red), and somatostatin (Sst, blue) shows altered numbers of hormone expressing cells in *Insm1* (F), *Neurod1* (G), and *Pax6* (H) KO mice. (I–L) Quantification of a percentage of hormone-positive cells among GFP-positive endocrine cells demonstrates defects in differentiation of cells positive for hormones: insulin (Ins) (I), glucagon (Gcg) (J), somatostatin (Sst) (K), and pancreatic polypeptide (Ppy) (L) in *Insm1*, *Neurod1*, and *Pax6* KO embryonic pancreata in comparison with *Insm1*$^{+/-}$. Error bars indicate SEM ($n = 3$); *P*-values were determined by one-way ANOVA test. Asterisks indicate *P*-values of *<0.05, **<0.01, and ***<0.001. Scale bars: 50 µm.

Etv4), cellular response to hormone stimulus (*Adra2a*, *Gcgr*, *Insr*, *Kcnc2*), hormone secretion (*Stxbkp5l*, *Stx1a*, *Cacna1d*), and mRNA metabolic process (*Srsf2*, *Hnrnpc*, *Celf4*, *Celf6*) (Supplementary Figure S4, D and F and Table S2).

Among the top URGs, there were many genes necessary for the key functions of mature islet cells. Examples include *Kcnc4* (Kv3.4), a voltage-gated potassium channel expressed in β- and δ-cells; and Gpr17, an orphan G protein-coupled receptor known to inhibit neural cell maturation (Gopel *et al.* 2000; Jacobson and Philipson 2007; Chen *et al.* 2009). GO and pathway enrichment analyses identified an enrichment in genes involved in the regulation of cellular component organization (*Adck1*, *Arap1*), Notch and Wnt signaling pathways (*Dll1*, *Notch1/2*, *Wnt7b*, *Frzb*, *Frz8*), and the negative regulation of cellular development (*Aatk*, *Dlx1*, *Rest*, *Kctd11*) (Supplementary Figure S4, E and F and Table S2). These results indicate that Insm1 stimulates many genes involved in hormone secretion and the function of mature endocrine cells, while repressing genes associated with Notch and Wnt signaling.

Dysregulated expression of genes involved in chromatin organization, cell proliferation, and mitochondrial function in *Neurod1* KO endocrine cells

Comparing the *Neurod1* KO and control datasets revealed a different set of 4613 dysregulated genes (2131 DRGs and 2482 URGs) (*P*-value ≤ 0.05) (Supplementary Figures S2D, S5, A and B and Table S1). The top DRGs included many factors known to impact islet

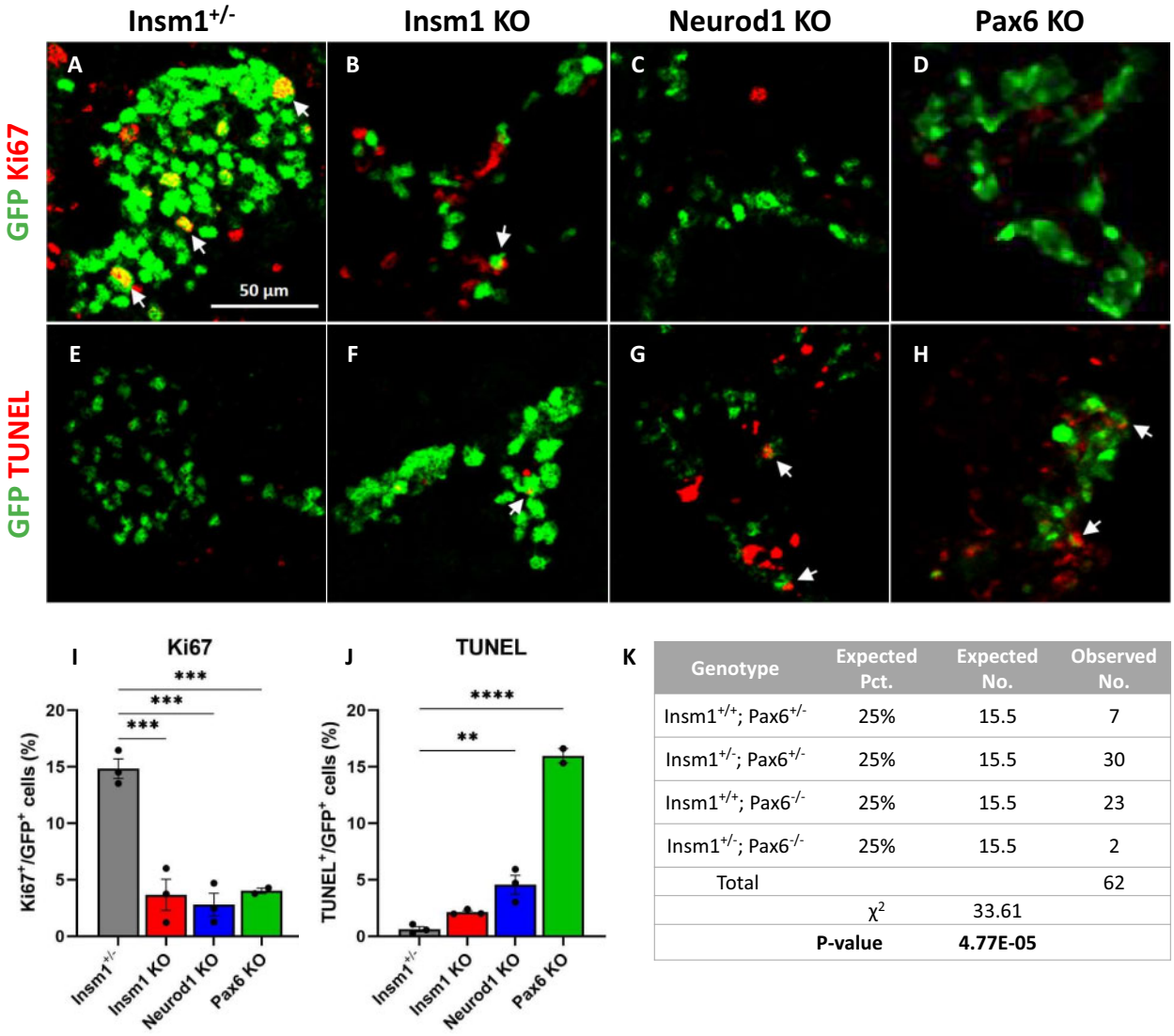

K

Genotype	Expected Pct.	Expected No.	Observed No.
Insm1$^{+/+}$; Pax6$^{+/-}$	25%	15.5	7
Insm1$^{+/-}$; Pax6$^{+/-}$	25%	15.5	30
Insm1$^{+/+}$; Pax6$^{-/-}$	25%	15.5	23
Insm1$^{+/-}$; Pax6$^{-/-}$	25%	15.5	2
Total			62
	χ^2	33.61	
	P-value	**4.77E-05**	

Figure 3 Decreased proliferation of endocrine cells in *Insm1*, *Neurod1*, and *Pax6* KOs, and increased apoptosis in *Neurod1* and *Pax6* KO embryos. (A–D) Immunofluorescence labeling of pancreatic tissues from E18.5 *Insm1*^{GFP}-expressing embryos using antibodies against GFP (green) that marks all pre-endocrine cells, and antibodies against cell proliferation marker Ki67 (red). Compared to controls (A), mice lacking *Insm1* (B), *Neurod1* (C), and *Pax6* (D) exhibit a decrease in the number of Ki67-positive endocrine cells. Arrows indicate cells co-expressing GFP and Ki67. (E–H) Immunofluorescence labeling of pancreatic tissues from E18.5 embryos with antibodies against GFP (green) and TUNEL assay (red) marking positive apoptotic events. Compared with *Insm1*$^{+/-}$ mice (E), mice lacking *Insm1* (F), *Neurod1* (G), and *Pax6* (H) exhibit an increase in the number of endocrine cells positive for both TUNEL and GFP. Arrows indicate TUNEL positive cells co-expressing GFP. (I) Quantification of a percentage of Ki67-positive cells among GFP-positive cells demonstrates a proliferation defect in endocrine cells from *Insm1*, *Neurod1*, and *Pax6* KO pancreata at E18.5. (J) Quantification of a percentage of TUNEL-positive cells among GFP-positive cells demonstrates increased apoptosis in endocrine cells in *Neurod1* and *Pax6* KO pancreata at E18.5. Error bars indicate SEM ($n = 3$); *P*-values were determined by one-way ANOVA test. Asterisks indicate *P*-values of *<0.05, **<0.01, and ***<0.001. Scale bars: 50 µm.

cell function, including *Prlr*, *G6pc2*, *Hspa1a*, and *Hspa1b* (Supplementary Figure S5C). Transcriptional co-regulators (*Runx1t1*, *Myt1l*), cell cycle regulation (*Cdkn1a*, *Cdc14b*), and chromatin organization (*Ctcf*, *Kat2b*) were enriched in DRGs in *Neurod1* KO (Supplementary Figure S5D and Table S2).

The top URGs in this dataset included the NF-κB signaling regulators (*Tifab*, *Ccdc3*), extracellular matrix factors (*Emilin2*, *Col19a1*), and the TRAIL receptor *Tnfsrf26* (Supplementary Figure S5C). URGs were enriched in such functional categories as cellular respiration (*Coq10a*, *Uqcc3*), mitochondrial organization (*Mfn2*, *Meif1*, *Meif2*, *Plekhf1*), and autophagy (*Atg7*, *Atg13*, *Tbc1d17*, *Vps11*) (Supplementary Figure S5D and Table S2). Moreover, genes involved in regulation of cell death were also upregulated (*P2rx1*, *P2rx7*, *C6*). Identification of these enriched GO terms and pathways for the *Neurod1* KO mice parallels the changes we and others have observed in islet morphology, including reduced endocrine cell proliferation and increased cell death (Naya *et al.* 1997; Romer *et al.* 2019). These findings indicate that the loss of *Neurod1* causes a transcriptional response marked by the upregulation of genes involved in NF-κB signaling and energy metabolism, and the downregulation of other pancreatic TFs and genes associated with cell cycle regulation.

Dysregulated expression of genes involved in cell cycle regulation, developmental growth, and apoptosis in *Pax6* KO endocrine cells

Comparison of the *Pax6* KO embryos and controls revealed a third set of 5770 genes (2756 DRGs and 3014 URGs) that were Pax6 dependent (*P*-value ≤ 0.05) (Supplementary Figures S2E, S6, A and B and Table S1). Among the top URGs were *Prlr*, *G6pc2*, *Gcg*, *Ptgdr*,

and *Ccdc3* (Supplementary Figure S6C). Inspection of the enriched GO terms and pathways for Pax6-dependent DRGs and URGs suggests a critical role for Pax6 in stimulating cell growth and cell cycle, and regulating endoplasmic reticulum (ER) stress and apoptosis in developing endocrine cells (Supplementary Figures S6, D and E and Table S2). Specifically, many genes involved in chromatin organization (*Ash1l*, *p300*, *Mettl4*), cell cycle regulation (*Ccnd1*, *Cdc27*, *Cdkn1b*, *Chek1*), and developmental cell growth (*Fgf9*, *Igf1r*, *Tgfb2*) were downregulated in *Pax6* KO animals (Supplementary Figure S6, D and F). Consistent with the diminished number of α-cells observed at E18.5, there was a marked reduction in *Gcg* expression, as well as dysregulation of other α-cell-specific genes *Brn4* and *Pcsk2*. GO terms and pathways enriched in URGs include cellular component organization (*Elmo1/2*, *Lima1*, *Myo7a*), response to ER stress (*Atf6b*, *Traf2*), and the apoptotic signaling pathway (*Casp2*, *Casp9*, *Madd*) (Supplementary Figure S6, E and F and TableS2). Analysis of dysregulated genes in *Pax6* KO animals shows the downregulation of other TFs, cell cycle regulators and genes important for cellular growth, and the upregulation of apoptotic signaling and genes involved in the response to ER stress.

Comparison of the gene sets dysregulated in the *Insm1*, *Neurod1*, and *Pax6* KO endocrine cells

To further assess the similarities and differences in the genes affected by each gene KO, we started by comparing the gene lists. We found that of the 8729 total dysregulated genes (based on adj. *P*-value ≤ 0.05) across all three KOs, 4719 (54%) were affected by more than one TF (Figures 4A and 5A). Additionally, 578 (6.6%) of genes were inversely regulated across TFs. For example, *Mnx1* is upregulated in *Pax6*- and *Neurod1* KO datasets and downregulated in *Insm1* KO samples, conversely *Rest* is downregulated in *Pax6*- and *Neurod1* KO samples and upregulated in *Insm1* KO data. Similarly, *Fev* is upregulated in the absence of *Pax6*, unchanged in *Neurod1* KO and downregulated in *Insm1* KO datasets (Supplementary Table S1). This finding indicates that while Insm1, Neurod1, and Pax6 commonly regulate a sizeable fraction of genes, each TF has unique effects on the transcriptome. To quantify these findings and reflect the similarity of the different groups, we determined the percentage of shared genes relative to the total number of dysregulated genes. This analysis revealed a range of 2.6–22.6% similarity between different groups, with the highest similarity between *Neurod1* and *Pax6* DRGs (22.6%).

Next, to identify commonalities in the functional annotations of genes dysregulated in each gene set, we performed Metascape analyses for both the DRGs and URGs. These analyses revealed many genes and functional GO terms and pathways shared between dysregulated genes from each gene set (Figures 4B and 5B). Of the 620 commonly regulated DRGs (14.07% shared), the enriched GO term and signaling pathway network includes such categories as regulation of mRNA metabolic processes and translation (*Akap17b*, *Clk1*, *Srsf3*, *Srsf6*), cell cycle regulation (*Bbx*, *Cdk6*, *Cdc14b*), and chromatin organization (*Kmt2a*, *Setd5*, *Kdm7a*) (Figure 4C and Supplementary Table S2). Other common DRGs included regulators of insulin secretion and signaling (*Ins1*, *Nnat*, *Ucn3*, *Insr*), transcriptional regulators (*St18*, *Neurod1*, *Rfx3*, *Myt1l*, *Runx1t1*, *Onecut2*), kinases (*Akt3*, *Mapk8*, *Taok1*, *Prkcb*), and anti-apoptotic genes (*Xiap*, *Bcl-W*) (Supplementary Table S1). While it is not surprising that these TFs regulate other TFs that are known to be involved in pancreas development and function, it is important to note their role in affecting the expression of cell cycle regulators and chromatin organization. Tight regulation of these processes has long been linked to cellular development, expansion, and differentiation, and their dysregulation likely contributes to the observed developmental delays and perturbed ratios of islet cell types (Dalton 2015; Kim *et al.* 2015; Boward *et al.* 2016; Soufi and Dalton 2016; Krentz *et al.* 2017).

The shared functional network for 863 URGs (17.7% shared) in all three KOs contains GO terms and pathways for ncRNA processing (*Aars*, *Ctu1*, *Lsm6*, *Tsen2*), apoptotic signaling pathway (*Casp9*, *Tradd*, *Tnfrsf21*, *Ddx47*), protein localization (*Ipo4*, *Ipo9*, *Timm29*), and response to oxidative stress (*Pink1*, *Selenon*, *Fancc*) (Figure 5C and Supplementary Table S2). Genes involved in Wnt-signaling pathways (*Frzb*, *Lzts2*) and other TFs (*Sox10*, *Tbx2*, *Foxa2*) were also upregulated (Supplementary Table S1). The upregulation of genes associated with apoptosis and oxidative stress response, in combination with the downregulation of anti-apoptotic genes, coincides with the increases in apoptosis in *Neurod1* and *Pax6* KO pancreata. Likewise, increases in the expression of members of the Wnt signaling pathway and early endocrine TFs are reminiscent of morphological developmental delays (Sharon *et al.* 2019). This is particularly true of those observed in *Insm1* KO embryos which are able to generate endocrine cells, but many of those are unable to properly differentiate and mature into hormone expressing endocrine cells (Mellitzer *et al.* 2006; Osipovich *et al.* 2014).

Metascape analysis also identified protein–protein interaction (PPI) enrichments common to all three gene sets. Enriched subnetworks of DRGs known to form PPIs included members of the ATF2- (*Atf2*, *Pou2f1*, *Nf1*, *Brca1*), cohesin- (*Smca1*, *Smc3*, *Atrx*, *Mecp2*), and histone acetylation-complexes (*Kat2b*, *Crebbp*, *Clock*). (Supplementary Figure S7, A, C, and E). The PPI subnetworks of URGs involved in NF-κB signaling (*Ikbkb*, *Ikbkg*, *Rnf31*, *Rbck1*) and histone modification (*Tuba1a, Hdac6, Kat5b*) (Supplementary Figure S8, A and C). Interestingly, NF-κB signaling has been recently shown to regulate β-cell proliferation and apoptosis, and in turn β-cell mass, during development (Sever *et al.* 2021). Together, these analyses indicate that while there are differences in the genes dysregulated by Insm1, Neurod1, and Pax6, there are many shared functionalities, both from a GO and PPI subnetwork perspective.

Prediction of direct targets of Insm1 and Neurod1 critical for endocrine cell development

To predict direct targets of Insm1 and Neurod1 in developing endocrine cells, we utilized previously reported ChIP-Seq datasets (Jia *et al.* 2015). Consistent with published data, our analysis showed that Insm1 and Neurod1 share a large proportion of binding sites (11,409 sites across the genome, 81.9% of total binding sites) (Supplementary Figure S9A). Integration of ChIP-Seq data with our RNA-Seq data on dysregulated genes suggests that 4180 and 3789 genes, respectively, may be direct targets of Insm1 and Neurod1 in endocrine progenitor cells (Supplementary Figure S9, B and C and Table S3). We further compared the lists of direct target genes and found 1,719 (27.5% shared) genes bound and dysregulated by both Insm1 and Neurod1. These included genes involved in peptide hormone response and secretion (*G6pc2*, *Glp1r*, *Sytl4*, *Stxbp5l*), zinc finger proteins (*Zfp326*, *Zbtb33*, *Zbdf2*), rhythmic processes (*Clock*, *Dhx9*, *Kcnd2*), and mRNA processing (*Celf4*, *Tra2a*, *Akap17b*, *Zfp871*, *Luc7l2*, *Ddx17*) (Supplementary Figure S9D). These findings indicate that of the genes dysregulated in our Insm1 and Neurod1 KO endocrine progenitor cells, 89% and 82% are predicted to be direct targets, respectively, based on the presence of binding sites within 5 kb of the transcriptional start site.

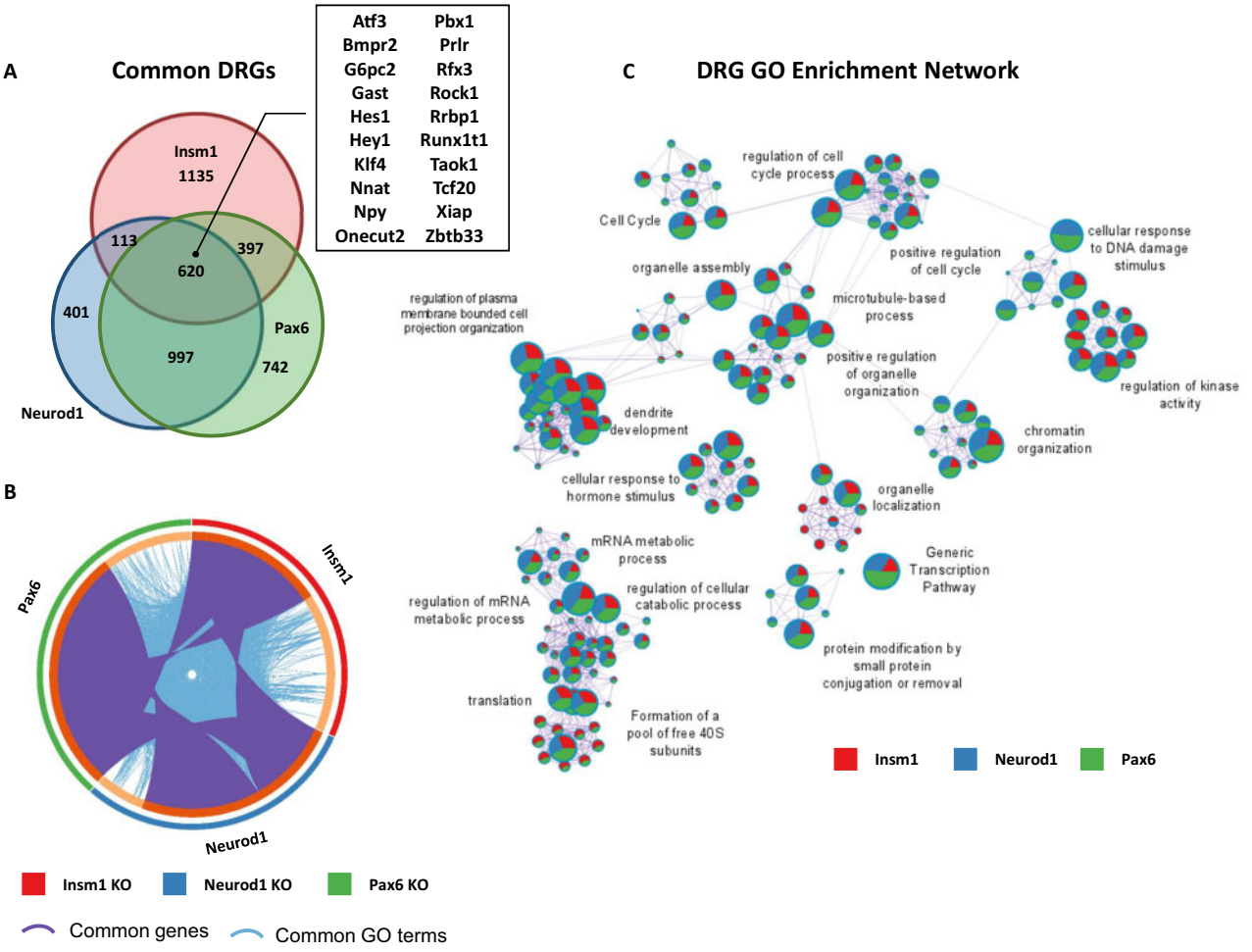

Figure 4 Enriched GO terms and pathways common for genes downregulated in *Insm1*, *Neurod1*, and *Pax6* KO pancreatic endocrine cells. (A) Venn diagram shows overlap between downregulated genes (DRGs) (*P*-value < 0.05 cutoff) in each of the pairwise comparisons: *Insm1* KO, *Neurod1* KO, and *Pax6*-KO versus *Insm1*$^{+/-}$ datasets. A subset of commonly downregulated genes is highlighted within a boxed insert. (B) Circos plot representing genes (purple curves) and GO terms/pathways (blue curves) that are shared between DRGs from the three comparisons. (C) Network depiction of the enriched gene ontology terms shared between DRGs from the three comparisons. Node size is proportional to the number of genes in GO or pathway category, with pie charts indicating a proportion of genes from each comparison in that GO term. Metascape analyses were run using default parameters.

Insm1, *Neurod1*, and *Pax6* KO endocrine cells exhibit dysregulated RNA splicing

Among the enriched GO terms and signaling pathways of dysregulated genes found in all three of the KO gene sets was the regulation of RNA metabolic processes, which includes the regulation of alternative splicing. To determine whether mRNA splicing was affected in the *Insm1*, *Neurod1*, and *Pax6* KO cells, we first examined the expression of several RBPs known to regulate mRNA splicing. We found several RBPs with similarly dysregulated expression patterns, including *Elavl3*, *Elavl4*, *Tra2A*, and *Tra2B* (Figure 6A). The expression of other differential RNA splicing factors such as serine/arginine-rich proteins that generally act as activators of splicing (*Srsf1*, *Srsf3*), heterogeneous nuclear ribonucleoproteins (hnRNPs) with repressive functions (*Hnrnpa0*, *Hnrnph1*, *Hnrnpha3*), and members of the spliceosome itself (*Sfb1*, *Sfb2*, *Sfb3*, *Sfb4*) are also dysregulated. Importantly, ChIP-Seq data indicate that Insm1 and Neurod1 bind at the promoter regions of many of the same RBPs whose expression levels are dysregulated in our KO data. For example, *Elavl3/4*, *Nova1*, *Tra2a/b*, and *Srsf1*, in addition to being downregulated, are all bound by both Insm1 and Neurod1 at their promoter regions (Supplementary Figure S10). To determine if the dysregulation of RBP expression in the absence of *Insm1*, *Neurod1*, or *Pax6* was correlated with differential splicing events, we used our RNA-Seq datasets to perform a computational alternative splicing analysis using JunctionSeq. The results indicated hundreds of differential splicing events in *Insm1* KO (356), *Neurod1* KO (212), and *Pax6* KO (885) datasets (adj. *P*-value ≤ 0.01, $\log_2$ FC > |1|) (Figure 6B and Supplementary Table S4). Of the 1,262 total differentially spliced genes, 172 were shared between pairs of TFs, with *Pax6* itself being alternatively spliced in Insm1 and Pax6 KO datasets (Supplementary Table S4). Additionally, *Tcf7l2*, which has strong polymorphism associations with T2D and is known to have isoform-specific effects on β-cell function, is also differentially spliced in the *Pax6* KO samples (Prokunina-Olsson, 2009; Osmark, 2009; Le Bacquer, 2011; Zhang, 2021). However, only 19 (1.5%) differential splicing events were common to all three KOs (*Ncoa4*, *Syt14*, *Tnfrsf12a*, *Mov10*) (Supplementary Table S4). Since some genes have several possible transcriptional isoforms, interpreting alternative splicing data is challenging. Therefore, we chose to take a closer look at a few genes that were differentially spliced in our KO datasets, and which have only a few RNA splicing variants.

Syt14 is a Ca^{2+}-independent synaptotagmin required for the exocytosis and trafficking of secretory vesicles. Interestingly differential splicing patterns were revealed for *Syt14* across all three

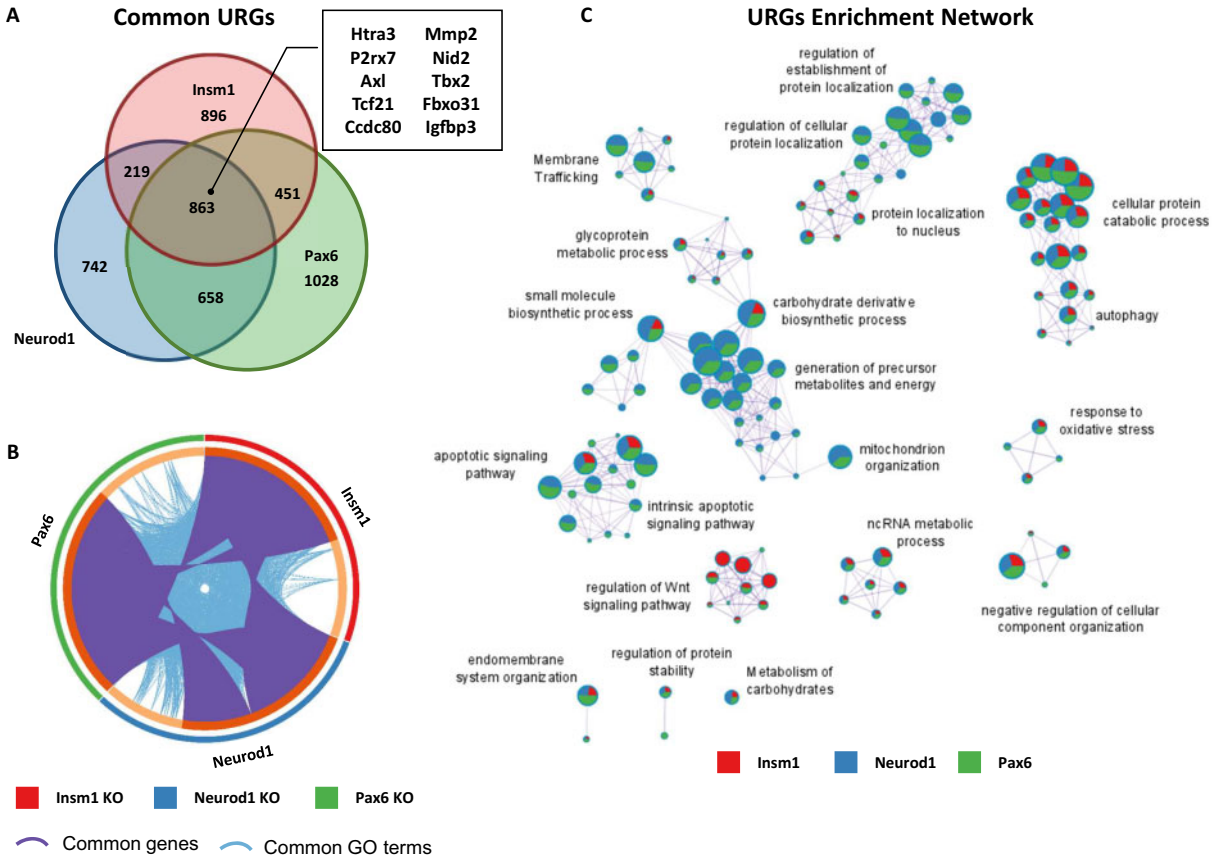

Figure 5 Enriched GO terms and pathways common for genes upregulated in *Insm1*, *Neurod1*, and *Pax6* KO pancreatic endocrine cells. (A) Venn diagram shows overlap between upregulated genes (URGs) (*P*-value < 0.05 cutoff) in each of the pairwise comparisons: *Insm1* KO, *Neurod1* KO, and *Pax6* KO versus *Insm1*$^{+/-}$ datasets. A subset of commonly downregulated genes is highlighted within a boxed insert. (B) Circos plot representing genes (purple curves) and GO terms/pathways (blue curves) that are shared between URGs from the three comparisons. (C) Network depiction of the enriched gene ontology terms shared between URGs from the three comparisons. Node size is proportional to the number of genes in GO or pathway category, with pie charts indicating a proportion of genes from each comparison in that GO term. Metascape analyses were run using default parameters.

KO datasets, specifically a decrease in expression of the Ensemble splice variant 205. To quantitatively visualize these differences, we generated splice junction plots (Sashimi plots), that tally the exon junction read counts. Sashimi plots of *Syt14* reveal a marked decrease of junction reads at exon 4 of the *Sty14*-205 splice variant (Figure 7A). To determine if dysregulated RBPs show binding preferences near the differentially spliced loci might cause these splicing differences, we used the online oRNAment database to identify local binding motifs (Benoit Bouvrette *et al.* 2020) and found that TRA2A, NOVA1, and ELAVL4 all show binding patterns at exon 4, as well as adjacent exons 3 and 5 (Figure 8A). Importantly, expression of *Tra2A* and *Elavl4* are downregulated in all three KO gene sets, and *Nova1* downregulated in *Pax6* KO suggesting their potential involvement in differential splicing of *Syt14* in developing endocrine cells (Figure 6A).

Similarly, *Snap* 25 is a critical SNARE protein involved in regulating exocytosis of synaptic vesicles in the brain and hormones in pancreatic islet cells (Kadkova *et al.* 2019; Liang *et al.* 2020). Two isoforms, *Snap25a* and *Snap25b*, have been identified that differ based on the alternative usage of two different exon 5 sequences (5a and 5b), with corresponding proteins differing in only 9 amino acids (Kadkova *et al.* 2019). We observe that the *Snap25b* isoform is increased in the *Pax6* KO (*P*-value < 0.001) and decreased in *Insm1* KO (*P*-value < 0.01) datasets, as indicated in the associated Sashimi plots (Figure 7B). RBP binding site analysis of this locus indicated TRA2A and NOVA1 binding sites at both 5a and 5b exons, and ELAVL4 sites at nearby upstream exons (Figure 8B). Together, these findings indicate that *Insm1*, *Neurod1*, and *Pax6* are required for the expression of RBPs that bind in the vicinity of exons whose proper splicing may be essential for the function of pancreatic endocrine cells.

Discussion

Insm1, *Neurod1*, and *Pax6* both independently and coordinately govern pre-endocrine cell gene expression

Insm1, *Neurod1*, and *Pax6* are individually essential for the formation of functional pancreatic endocrine cells (Naya *et al.* 1997; St-Onge *et al.* 1997; Gierl *et al.* 2006; Gu *et al.* 2010; Osipovich *et al.* 2014; Jia *et al.* 2015; Mitchell *et al.* 2017). Here, we systematically compared the effects of deleting *Insm1*, *Neurod1*, and *Pax6* in a *Insm1*^{GFPCre} heterozygous background based on the morphology, gene expression, and differential RNA splicing of nascent pancreatic endocrine cells. By doing so, we obtained new insights into the vital roles that each of these factors has in the development of pancreatic endocrine cells.

Role of *Insm1*

Consistent with previously published results we showed that Insm1 KOs have defects in endocrine cell differentiation that were manifested in decreased numbers of Ins- and Gcg-positive

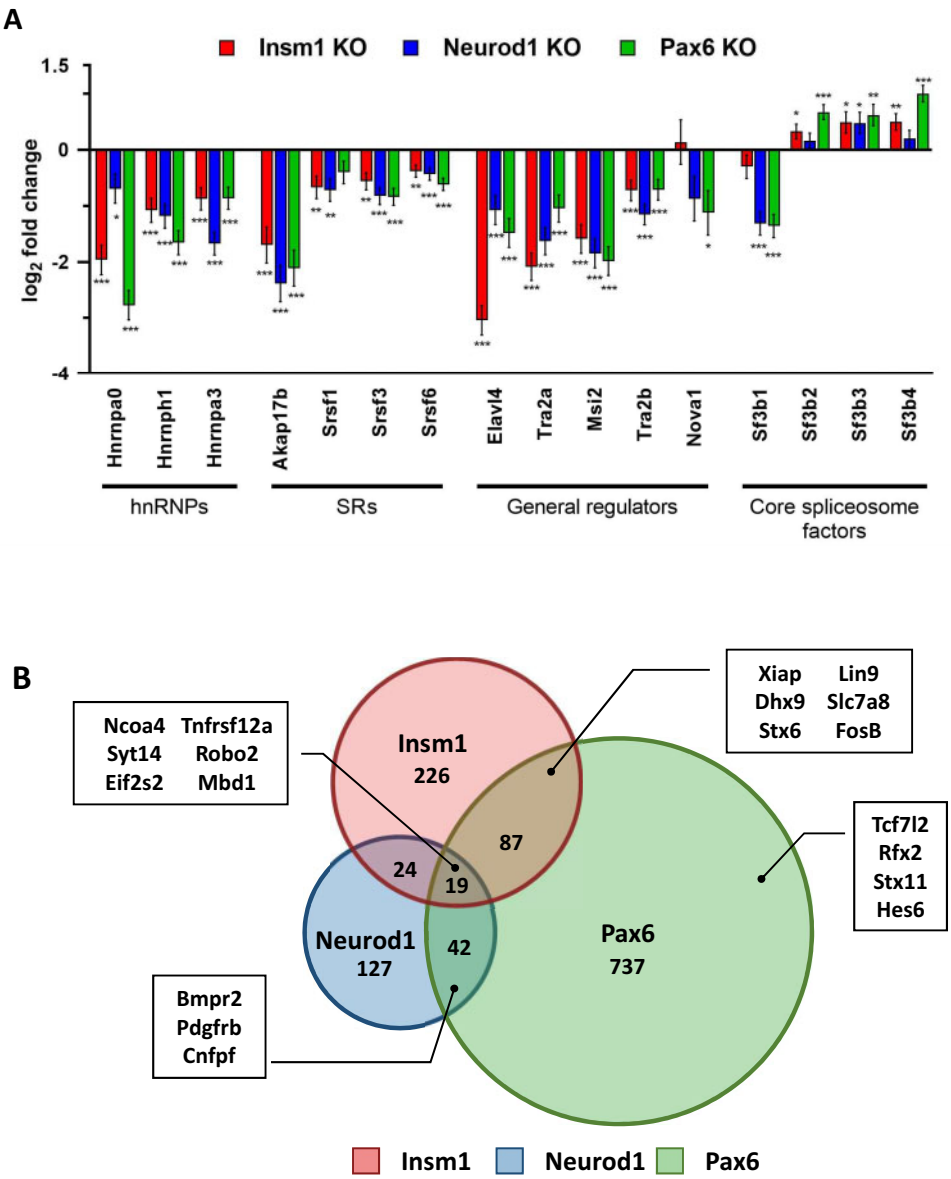

Figure 6 *Insm1*, *Neurod1*, and *Pax6* regulate alternative splicing in pancreatic endocrine cells. (A) Many important RNA binding proteins (RBPs) are dysregulated in in *Insm1*, *Neurod1*, and *Pax6* KOs. Bar graph of the $\log_2$ fold change of a subset of dysregulated RBPs. Asterisks indicate *P*-values of *<0.05, **<0.01, ***<0.001. (B) Venn diagram demonstrates overlaps between differentially spliced genes in *Insm1*, *Neurod1*, and *Pax6* KO RNA-Seq datasets. Examples of alternatively spliced genes are highlighted with a box insert. Differential splicing events between the knock-out and control groups were identified by performing JunctionSeq analysis on the RNA-Seq datasets. A cutoff of *P*-adj. value ≤0.01 and $\log_2$ fold change ≥|1| was used.

and increased number of Ppy-positive endocrine cells. This is accompanied by decreased endocrine cell proliferation, as well as changes in expression of genes that affect these processes (Gierl *et al.* 2006; Osipovich *et al.* 2014). Our comparative transcriptional analysis revealed both similarities and differences in the genes regulated by Insm1 and Neurod1 and Pax6. For example, Insm1, but not Neurod1 or Pax6, activates the expression of *Fev* and *Mnx1* in endocrine cells, TFs that are known to influence the numbers and types of endocrine cells, as well as islet morphology. Insm1 is specifically important for expression of many genes involved in inducible secretory function of endocrine cells, including protein secretion and Ca^{2+} regulated vesicle exocytosis. This is consistent with the role of *Insm1* in the proliferative and secretory functions of mature endocrine cells (Tao *et al.*, 2018). Our new data, together with re-analysis of previously reported ChIP-Seq data, suggests that 89% of genes dysregulated in endocrine progenitor cells of Insm1 KO mice contain binding sites for Insm1 with 5 kb of the transcriptional start site.

Role of *Neurod1*

Mice that lack *Neurod1* exhibit an increased number of Ppy-expressing endocrine cells without significantly altering the proportion of other differentiated endocrine cell types. However, *Neurod1* KO mice exhibit both a profound decrease in proliferation and an increase in apoptosis of endocrine cells, thereby causing a marked reduction in overall number of endocrine cells. These findings are consistent with previous studies, supporting the hypothesis that a lack of proliferative cells and increase in apoptosis are primary causes for the reduced total number of endocrine cells observed (Naya *et al.* 1997; Romer *et al.* 2019). Likewise, Romer *et al.* (2019) recently reported a decrease in α- and β-cell numbers only after the time ∼P0 stage. Their quantifications at

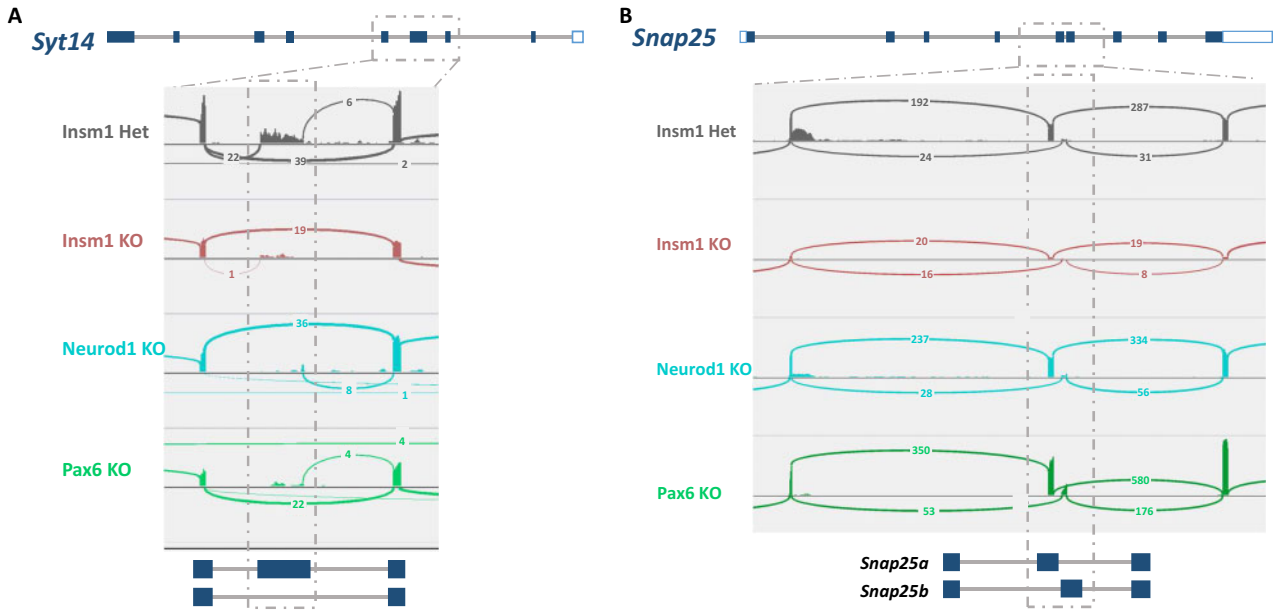

Figure 7 Identification of differential splicing events in *Syt14* and *Snap25* genes. The gene structures of (A) *Syt14* and (B) *Snap25* are illustrated above corresponding Sashimi plots of differentially spliced regions. Sashimi plots show the representative splice junctions as arcs that connect the exons in each of the datasets. The numbers found on each of the corresponding arcs indicate the junction depth, or reads spanning the exon junctions. Dashed boxes highlight the regions of alternative splicing, which are again depicted below the Sashimi plot to provide a visual reference for read alignments. Sashimi plots were generated using the Integrated Genomic Viewer (IGV).

E17 show no differences in the cell numbers or ratios of Ins- or Gcg-expressing cells, indicating that the specific reduction in α- and β-cells occurs during late embryonic to early postnatal stages after islet differentiation has largely concluded, which is consistent with our findings.

Our transcriptional profiling results also suggest that *Neurod1* promotes proliferation and maturation through the stimulation of genes important for cell cycle regulation and chromatin modifications, processes that are important for cell differentiation and function (Pauklin and Vallier 2013; Chen and Dent 2014; Dowen *et al.* 2014; Krentz *et al.* 2017). Simultaneously, the observed upregulation of apoptotic and autophagy genes likely contributes to an increase in cell death, further decreasing the total number of endocrine cells.

The regulation of endocrine specific TFs (*Fev*, *Mnx1*) and other genes important for cellular function further support a role for Neurod1 in mature cells as is suggested both by the expression of Neurod1 in adult β- and α-cells and that the conditional ablation of Neurod1 in β-cells impairs their maturation (Naya *et al.* 1997; Gu *et al.* 2010; Mastracci *et al.* 2013). Additionally, ChIP-Seq data indicates that Neurod1 binds within 5 kb of 82% of the genes dysregulated in this analysis, strongly suggesting that it is the primary effector of the observed changes. Together these findings indicate the critical role of Neurod1 in propagating enough fully functional islet cells during development via the promotion of cellular proliferation and activation of key TFs.

Role of *Pax6*

It is well established that Pax6 is necessary for the specification of pancreatic α-cells, so the marked reduction of Gcg-positive cells (3.3% vs. 15% in controls) in the *Pax6* KO animals is not a surprise (Gosmain *et al.* 2010). However, our data have revealed that endocrine cells lacking *Pax6* not only have a decrease in the expression of *Gcg*, but also a marked dysregulation of other genes important for α-cell development and function, such as *Pou3f4* (or *Brn4*), *Pcsk2*, *Slc30a8*, *Irx2*, and *Smarca1*. Besides its function in α-cells, Pax6 is important for development and function of adult β-cells, which is supported by our findings of decreased expression of *Ins1*, *Ins2*, and *Insr* in Pax6 KOs (Gosmain *et al.* 2012; Mitchell *et al.* 2017; Swisa *et al.* 2017). While the morphological phenotypes of the islets we observed are in line with previously published results, due to the design of our study we cannot exclude a combinatorial effect caused by the haplosufficiency of *Insm1* in mice containing the $Insm1^{GFPCre}$ allele (Sander *et al.* 1997; St-Onge *et al.* 1997; Gosmain *et al.* 2010). Indeed, and as discussed below, the difficulty we had in obtaining *Pax6* KO animals at E18.5, which contained only one $Insm1^{GFPCre}$ allele, could be due defects in the developing central nervous system where both Pax6 and *Insm1* are expressed (Farkas *et al.* 2008; Lan and Breslin 2009; Osipovich *et al.* 2014). Furthermore, it was previously shown that Pax6 RNA is alternatively spliced, and that β- and α-cells preferably express different splicing variants (Singer *et al.* 2019). Thus, our finding that Insm1 affects the processing of *Pax6* mRNA also affects the interpretation of our results. Despite this, the downregulation of genes involved in chromatin organization, cell cycle regulation, and cell growth in the *Pax6* KOs, similar to *Neurod1* KOs, likely contributes to the reduction in endocrine cell expansion, while an increase in apoptotic genes correlates to the increase in cell death.

Regulatory overlap of *Insm1*, *Neurod1*, and *Pax6*

Recently, we have shown that *Insm1* and *Neurod1* exhibit a high degree of co-expression during endocrine differentiation, and that *Pax6* is similar except that it continues to be expressed in adult β-cells (Osipovich *et al.* 2021). These co-expression relationships are consistent with *Insm1*, *Neurod1*, and *Pax6* being important components of the GRN in nascent pancreatic endocrine cells. The genes regulated by these three factors also share many functional assignments, such as mRNA processing and alternative splicing and cell cycle regulation. These similarities likely underpin the broadly similar morphological phenotypes when each is knocked-out, which includes a reduced overall number of pro-

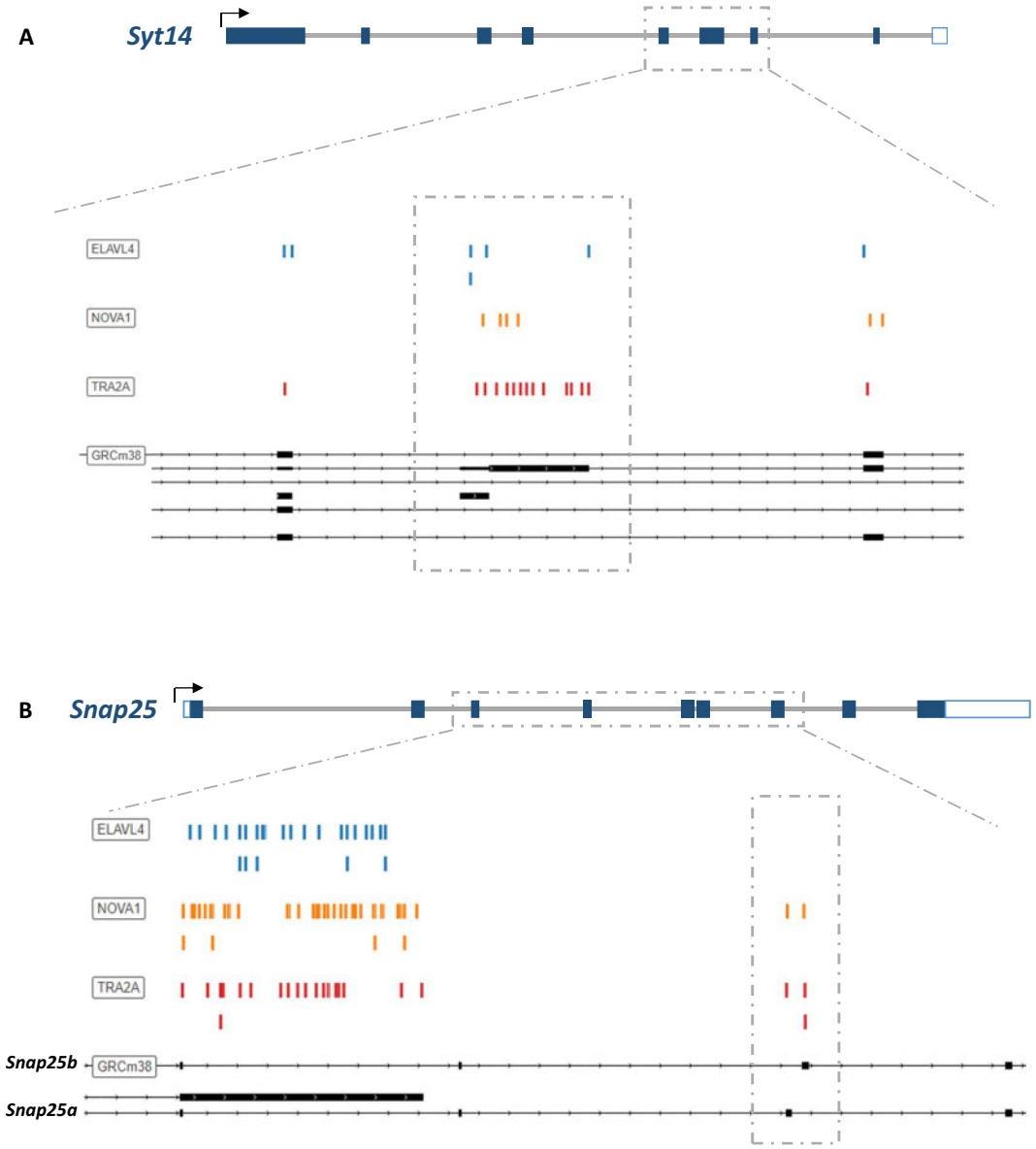

Figure 8 Differentially spliced regions of *Syt14* and *Snap25* genes are bound by dysregulated RBPs. (A) Schematic of *Syt14* gene structure and corresponding binding sites of the RBPs ELAVL4, NOVA1, and TRA2A near the differentially spliced regions. (B) Schematic of *Snap25* and corresponding binding sites of ELAVL4, NOVA1, and TRA2A at the differentially spliced site. Colored dashes above the indicated gene region represent the putative binding site of the given RPB. Binding sites were identified via the online oRNAment database.

endocrine cells, reduced endocrine cell proliferation and increased apoptosis, as well as defects in differentiation toward different kinds of hormone-expressing cells.

Our findings strongly point to a negative epistasis between *Insm1* and *Pax6*, as already noted, due to the fewer than expected numbers of $Insm1^{GFPCre/+}$; $Pax6^{fl/fl}$ animals at E18.5. Consistent with this, a recent report showed that mice with only a single functional *Insm1* allele ($Insm1^{+/-}$) have impaired β-cell proliferation that results in impaired glucose tolerance in adult animals (Tao *et al.* 2018). However, the authors observed no impairments in β-cell mass at birth and argued that *Insm1* haploinsufficiency has little to no effect on embryonic endocrine development (Tao *et al.* 2018). Previous *Pax6* KO studies have also not reported any unexpected difficulties in obtaining *Pax6* null embryos, and animals died just after birth (Sander *et al.* 1997; St-Onge *et al.* 1997; Ashery-Padan *et al.* 2004; Heller *et al.* 2004). Nonetheless, the reduced number of *Pax6* KO embryos at E18.5 appears to be due to a detrimental synergistic effect, or negative epistasis, between *Insm1* and *Pax6* that impairs embryo survival.

In addition to the greater lethality of *Pax6* KO embryos, our data show an increase in both apoptotic events at E18.5, an increase in expression of pro-apoptotic genes and a decrease in expression of anti-apoptotic genes at E15.5. Previous studies of global *Pax6* KO mice have all observed a marked decrease in hormone-positive endocrine cells, but none quantified apoptosis events (Sander *et al.* 1997; St-Onge *et al.* 1997; Ashery-Padan *et al.* 2004; Heller *et al.* 2004). Moreover, Ashery-Padan *et al.* (2004), who utilized a Cre-Lox-based lineage tracing strategy to quantify the proportion of *Pax6* expressing cells relative to total pancreatic tissue at E18.5, reported the loss of hormone expression but no difference in total cell number. While apoptosis was not specifically quantified, their study suggests that pro-endocrine cells form and expand but then fail only to express islet hormones (Ashery-Padan *et al.* 2004). If so, then our observations are consistent with

Insm1 and *Pax6* having redundant functions, perhaps in the suppression pro-apoptotic genes. In the future, alternate strategies that do not rely on the *Insm1*^{GFPCre} the allele and that maintain full expression of *Insm1* will need to be utilized to explore how these two genes interact with each other.

Dysregulation of RBP gene expression and identification of alternative splicing events in Insm1, Neurod1, and Pax6 KO animals

Alternative RNA splicing enables a single gene to give rise to multiple mRNA products that encode different protein products. The function of these different protein products can vary greatly and impact cellular function (Alvelos *et al.* 2018). Recent studies have suggested the importance of the unique splicing program innate to pro-endocrine cells, and how the functional outputs help steer the developmental process, yet it remains incompletely understood (Juan-Mateu *et al.* 2018; Singer *et al.* 2019; Colli *et al.* 2020; Alvelos *et al.* 2021).

Our analyses indicate Insm1, Neurod1, and Pax6 each regulate the expression of RBPs that mediate different RNA splicing events, including expression of *Elavl4*, *Tra2A*, *Msi1* and *Msi2*, and *Nova1*. Consistent with this, we identified multiple global differential slicing events within KO datasets and, specifically, in the *Syt14* and *Snap25* genes. Synaptotagmin 14 (*Syt14*) is a member of the SYT family that is necessary for exocytosis of secretory vesicles, and mutations in this gene have been associated with neurodegenerative disorders in humans (Doi *et al.* 2011). Our data revealed that *Syt14* is differentially spliced in all three of the KO mice studied. Similarly, Synaptosome Associated Protein 25, or *Snap25*, is a member of the SNARE complex. It is necessary for insulin secretion, is known to be downregulated in T2D islet cells, and is differentially spliced in both *Insm1* and *Pax6* KO endocrine cells (Sadoul *et al.* 1995; Gonelle-Gispert *et al.* 1999; Ostenson *et al.* 2006; Daraio *et al.* 2017). It is well established that *Snap25* has two primary mRNA isoforms that have slightly different localization patterns and functional traits (Nagy *et al.* 2005; Daraio *et al.* 2017; Irfan *et al.* 2019). Considering this information, it is likely that the differential splicing of these both *Syt14* and *Snap25* contributes to the impaired function of KO islets. Moreover, it also highlights the importance of alternative splicing in endocrine cell development and indicate that *Insm1*, *Neurod1*, and *Pax6*, besides having large effects on the transcriptome, also control differential splicing events through their regulation of RBPs and thereby affect endocrine cell function in this manner. In the future, it would be beneficial to determine the effects of disrupting the TF binding sites at the promoter regions of RBPs on gene expression levels. Likewise, more work needs to be done to determine the role of specific binding activity of RBPs at their target sites within alternatively spliced genes and if those RBPs maintain endocrine-specific functions.

In conclusion, the present study provides additional insights into the roles for Insm1, Neurod1, and Pax6 in driving endocrine development and differentiation. While each of these TFs has its own unique regulatory functions, there is also functional overlap between these factors based on the large number of commonly dysregulated genes represented in our data. Importantly, we show that the differential expression of RBPs correlates with differential splicing events that can either be shared or common to each gene KO, demonstrating a novel role shared by each factor. Finally, our data demonstrate the broad impact of eliminating each TF, further illustrating their individual roles and importance in establishing the GRN within pancreatic endocrine cells.

Data availability

RNA sequencing data are available at ArrayExpress with the accession number E-MTAB-10262. The authors affirm that all data necessary for confirming the conclusions of the article are present within the article, figures, and tables provided.

Supplementary material is available at *G3* online.

Acknowledgments

We thank the staff of both the Vanderbilt Cell Imaging Shared Resource and the Vanderbilt Technologies for Advanced Genomics (VANTAGE) for their expert assistance.

Funding

This study was supported by funding from the National Institutes of Health to MAM (DK72473 and DK89523), to VANTAGE (CA68485, EY08126, and RR030956), and to the Vanderbilt Cell Imaging Shared Resource (CA68485, DK20593, DK58404, DK59637, and EY08126). K.D.D. received support from the Molecular Endocrinology Training Program (T32 DK07563).

Conflicts of interest

The authors declare that there is no conflict of interest.

Author contribution

K.D.D. and A.B.O. performed experiments and analyzed data. J.P.C. performed RNA-Seq data processing, alignment, and differential expression analyses. K.D.D., A.B.O., and M.A.M. wrote and edited the manuscript. M.A.M. supervised the experiments.

Literature cited

Alvelos MI, Bruggemann M, Sutandy FR, Juan-Mateu J, Colli ML, *et al.* 2021. The RNA-binding profile of the splicing factor SRSF6 in immortalized human pancreatic β-cells. Life Sci Alliance. 4: e202000825.

Alvelos MI, Juan-Mateu J, Colli ML, Turatsinze JV, Eizirik DL. 2018. When one becomes many-alternative splicing in beta-cell function and failure. Diabetes Obes Metab. 20 (Suppl 2):77–87.

Anders S, Pyl PT, Huber W. 2015. HTSeq—a python framework to work with high-throughput sequencing data. Bioinformatics. 31: 166–169.

Arda HE, Benitez CM, Kim SK. 2013. Gene regulatory networks governing pancreas development. Dev Cell. 25:5–13.

Ashery-Padan R, Marquardt T, Zhou X, Gruss P. 2000. *Pax6* activity in the lens primordium is required for lens formation and for correct placement of a single retina in the eye. Genes Dev. 14: 2701–2711.

Ashery-Padan R, Zhou X, Marquardt T, Herrera P, Toube L, *et al.* 2004. Conditional inactivation of *Pax6* in the pancreas causes early onset of diabetes. Dev Biol. 269:479–488.

Bechard ME, Bankaitis ED, Hipkens SB, Ustione A, Piston DW, *et al.* 2016. Precommitment low-level *Neurog3* expression defines a long-lived mitotic endocrine-biased progenitor pool that drives production of endocrine-committed cells. Genes Dev. 30: 1852–1865.

Benoit Bouvrette LP, Bovaird S, Blanchette M, Lecuyer E. 2020. Ornament: a database of putative RNA binding protein target

sites in the transcriptomes of model species. Nucleic Acids Res. 48:D166–D173.

Boward B, Wu T, Dalton S. 2016. Concise review: control of cell fate through cell cycle and pluripotency networks. Stem Cells. 34: 1427–1436.

Burlison JS, Long Q, Fujitani Y, Wright CV, Magnuson MA. 2008. *Pdx1* and *Ptf1a* concurrently determine fate specification of pancreatic multipotent progenitor cells. Dev Biol. 316:74–86.

Carazo F, Romero JP, Rubio A. 2019. Upstream analysis of alternative splicing: a review of computational approaches to predict context-dependent splicing factors. Brief Bioinform. 20: 1358–1375.

Chen T, Dent SY. 2014. Chromatin modifiers and remodellers: regulators of cellular differentiation. Nat Rev Genet. 15:93–106.

Chen Y, Wu H, Wang S, Koito H, Li J, *et al.* 2009. The oligodendrocyte-specific G protein-coupled receptor GPR17 is a cell-intrinsic timer of myelination. Nat Neurosci. 12:1398–1406.

Choi E, Kraus MR, Lemaire LA, Yoshimoto M, Vemula S, *et al.* 2012. Dual lineage-specific expression of *Sox17* during mouse embryogenesis. Stem Cells. 30:2297–2308.

Colli ML, Ramos-Rodriguez M, Nakayasu ES, Alvelos MI, Lopes M, *et al.* 2020. An integrated multi-omics approach identifies the landscape of interferon-alpha-mediated responses of human pancreatic beta cells. Nat Commun. 11:2584.

Dalton S. 2015. Linking the cell cycle to cell fate decisions. Trends Cell Biol. 25:592–600.

Daraio T, Bombek LK, Gosak M, Valladolid-Acebes I, Klemen MS, *et al.* 2017. SNAP-25b-deficiency increases insulin secretion and changes spatiotemporal profile of Ca^{2+} oscillations in β cell networks. Sci Rep. 7:7744.

Dobin A, Davis CA, Schlesinger F, Drenkow J, Zaleski C, *et al.* 2013. STAR: Ultrafast universal RNA-seq aligner. Bioinformatics. 29: 15–21.

Doi H, Yoshida K, Yasuda T, Fukuda M, Fukuda Y, *et al.* 2011. Exome sequencing reveals a homozygous SYT14 mutation in adult-onset, autosomal-recessive spinocerebellar ataxia with psychomotor retardation. Am J Hum Genet. 89:320–327.

Dowen JM, Fan ZP, Hnisz D, Ren G, Abraham BJ, *et al.* 2014. Control of cell identity genes occurs in insulated neighborhoods in mammalian chromosomes. Cell. 159:374–387.

Ejarque M, Cervantes S, Pujadas G, Tutusaus A, Sanchez L, *et al.* 2013. *Neurogenin3* cooperates with *Foxa2* to autoactivate its own expression. J Biol Chem. 288:11705–11717.

Farkas LM, Haffner C, Giger T, Khaitovich P, Nowick K, *et al.* 2008. *Insulinoma-associated 1* has a panneurogenic role and promotes the generation and expansion of basal progenitors in the developing mouse neocortex. Neuron. 60:40–55.

Fiszbein A, Kornblihtt AR. 2017. Alternative splicing switches: important players in cell differentiation. Bioessays. 39:1600157.

Gierl MS, Karoulias N, Wende H, Strehle M, Birchmeier C. 2006. The zinc-finger factor *Insm1* (IA-1) is essential for the development of pancreatic beta cells and intestinal endocrine cells. Genes Dev. 20:2465–2478.

Gonelle-Gispert C, Halban PA, Niemann H, Palmer M, Catsicas S, *et al.* 1999. SNAP-25a and -25b isoforms are both expressed in insulin-secreting cells and can function in insulin secretion. Biochem J. 339 (Pt 1):159–165.

Gopel SO, Kanno T, Barg S, Rorsman P. 2000. Patch-clamp characterisation of somatostatin-secreting cells in intact mouse pancreatic islets. J Physiol. 528:497–507.

Gosmain Y, Katz LS, Masson MH, Cheyssac C, Poisson C, *et al.* 2012. *Pax6* is crucial for beta-cell function, insulin biosynthesis, and glucose-induced insulin secretion. Mol Endocrinol. 26:696–709.

Gosmain Y, Marthinet E, Cheyssac C, Guerardel A, Mamin A, *et al.* 2010. *Pax6* controls the expression of critical genes involved in pancreatic {alpha} cell differentiation and function. J Biol Chem. 285:33381–33393.

Gradwohl G, Dierich A, LeMeur M, Guillemot F. 2000. *Neurogenin3* is required for the development of the four endocrine cell lineages of the pancreas. Proc Natl Acad Sci USA. 97:1607–1611.

Gu C, Stein GH, Pan N, Goebbels S, Hornberg H, *et al.* 2010. Pancreatic beta cells require *Neurod* to achieve and maintain functional maturity. Cell Metab. 11:298–310.

Gu G, Dubauskaite J, Melton DA. 2002. Direct evidence for the pancreatic lineage: *Ngn3*+ cells are islet progenitors and are distinct from duct progenitors. Development. 129:2447–2457.

Heller RS, Stoffers DA, Liu A, Schedl A, Crenshaw EB 3rd, *et al.* 2004. The role of *Brn4/Pou3f4* and *Pax6* in forming the pancreatic glucagon cell identity. Dev Biol. 268:123–134.

Huang da W, Sherman BT, Lempicki RA. 2009a. Bioinformatics enrichment tools: paths toward the comprehensive functional analysis of large gene lists. Nucleic Acids Res. 37:1–13.

Huang da W, Sherman BT, Lempicki RA. 2009b. Systematic and integrative analysis of large gene lists using DAVID bioinformatics resources. Nat Protoc. 4:44–57.

Huang HP, Liu M, El-Hodiri HM, Chu K, Jamrich M, *et al.* 2000. Regulation of the pancreatic islet-specific gene *Beta2* (*Neurod*) by *neurogenin* 3. Mol Cell Biol. 20:3292–3307.

Irfan M, Gopaul KR, Miry O, Hokfelt T, Stanton PK, *et al.* 2019. SNAP-25 isoforms differentially regulate synaptic transmission and long-term synaptic plasticity at central synapses. Sci Rep. 9: 6403.

Jacobson DA, Philipson LH. 2007. Action potentials and insulin secretion: new insights into the role of K_v channels. Diabetes Obes Metab. 9 (Suppl 2):89–98.

Jeffery N, Richardson S, Chambers D, Morgan NG, Harries LW. 2019. Cellular stressors may alter islet hormone cell proportions by moderation of alternative splicing patterns. Hum Mol Genet. 28: 2763–2774.

Jia S, Ivanov A, Blasevic D, Muller T, Purfurst B, *et al.* 2015. *Insm1* cooperates with *Neurod1* and *Foxa2* to maintain mature pancreatic beta-cell function. EMBO J. 34:1417–1433.

Juan-Mateu J, Alvelos MI, Turatsinze JV, Villate O, Lizarraga-Mollinedo E, *et al.* 2018. *Srp55* regulates a splicing network that controls human pancreatic beta-cell function and survival. Diabetes. 67:423–436.

Kadkova A, Radecke J, Sorensen JB. 2019. The SNAP-25 protein family. Neuroscience. 420:50–71.

Kim YH, Larsen HL, Rue P, Lemaire LA, Ferrer J, Grapin-Botton A. 2015. Cell cycle-dependent differentiation dynamics balances growth and endocrine differentiation in the pancreas. PLoS Biol. 13:e1002111.

Krentz NAJ, van Hoof D, Li Z, Watanabe A, Tang M, *et al.* 2017. Phosphorylation of *Neurog3* links endocrine differentiation to the cell cycle in pancreatic progenitors. Dev Cell. 41:129–142.e6.

Lan MS, Breslin MB. 2009. Structure, expression, and biological function of *Insm1* transcription factor in neuroendocrine differentiation. FASEB J. 23:2024–2033.

Le Bacquer O, Shu L, Marchand M, Neve B, Paroni F, *et al.* 2011. TCF7L2 splice variants have distinct effects on beta-cell turnover

and function. Hum Mol Genet. 20:1906–1915. doi: 10.1093/hmg/ddr072. Epub 2011 Feb 28. PMID: 21357677.

Liang T, Qin T, Kang F, Kang Y, Xie L, *et al.* 2020. SNAP23 depletion enables more SNAP25/calcium channel excitosome formation to increase insulin exocytosis in type 2 diabetes. JCI Insight. 5: e129694.

Licatalosi DD, Darnell RB. 2010. RNA processing and its regulation: global insights into biological networks. Nat Rev Genet. 11:75–87.

Lizio M, Ishizu Y, Itoh M, Lassmann T, Hasegawa A, *et al.*; FANTOM consortium. 2015. Mapping mammalian cell-type-specific transcriptional regulatory networks using KD-CAGE and ChIP-seq Data in the TC-YIK cell line. Front Genet. 6:331.

Love MI, Huber W, Anders S. 2014. Moderated estimation of fold change and dispersion for RNA-seq data with DESeq2. Genome Biol. 15:550.

Manning KS, Cooper TA. 2017. The roles of RNA processing in translating genotype to phenotype. Nat Rev Mol Cell Biol. 18:102–114.

Mastracci TL, Anderson KR, Papizan JB, Sussel L. 2013. Regulation of *Neurod1* contributes to the lineage potential of *Neurogenin3*+ endocrine precursor cells in the pancreas. PLoS Genet. 9:e1003278.

McDonald E, Li J, Krishnamurthy M, Fellows GF, Goodyer CG, *et al.* 2012. *Sox9* regulates endocrine cell differentiation during human fetal pancreas development. Int J Biochem Cell Biol. 44:72–83.

Mellitzer G, Bonne S, Luco RF, Van De Casteele M, Lenne-Samuel N, *et al.* 2006. *IA1* is *NGN3*-dependent and essential for differentiation of the endocrine pancreas. EMBO J. 25:1344–1352.

Mitchell RK, Nguyen-Tu MS, Chabosseau P, Callingham RM, Pullen TJ, *et al.* 2017. The transcription factor *Pax6* is required for pancreatic beta cell identity, glucose-regulated ATP synthesis, and Ca dynamics in adult mice. J Biol Chem. 292:8892–8906.

Miyata T, Maeda T, Lee JE. 1999. *Neurod* is required for differentiation of the granule cells in the cerebellum and hippocampus. Genes Dev. 13:1647–1652.

Nagy G, Milosevic I, Fasshauer D, Muller EM, de Groot BL, *et al.* 2005. Alternative splicing of SNAP-25 regulates secretion through nonconservative substitutions in the snare domain. Mol Biol Cell. 16: 5675–5685.

Naya FJ, Huang HP, Qiu Y, Mutoh H, DeMayo FJ, *et al.* 1997. Diabetes, defective pancreatic morphogenesis, and abnormal enteroendocrine differentiation in *Beta2/Neurod*-deficient mice. Genes Dev. 11:2323–2334.

Osipovich AB, Dudek KD, Greenfest-Allen E, Cartailler J, Manduchi E, *et al.* 2021. A developmental lineage-based gene co-expression network for mouse pancreatic β-cells reveals a role for *Zfp800* in pancreas development. Development. 148:dev196964.

Osmark P, Hansson O, Jonsson A, Rönn T, Groop L, *et al.* 2009. Unique splicing pattern of the TCF7L2 gene in human pancreatic islets. Diabetologia. 52:850–854. doi: 10.1007/s00125-009-1293-z. Epub 2009 Feb 27. PMID: 19247628.

Osipovich AB, Long Q, Manduchi E, Gangula R, Hipkens SB, *et al.* 2014. *Insm1* promotes endocrine cell differentiation by modulating the expression of a network of genes that includes *Neurog3* and *Ripply3*. Development. 141:2939–2949.

Ostenson CG, Gaisano H, Sheu L, Tibell A, Bartfai T. 2006. Impaired gene and protein expression of exocytotic soluble n-ethylmaleimide attachment protein receptor complex proteins in pancreatic islets of type 2 diabetic patients. Diabetes. 55:435–440.

Pan FC, Brissova M, Powers AC, Pfaff S, Wright CV. 2015. Inactivating the permanent neonatal diabetes gene *Mnx1* switches insulin-producing beta-cells to a delta-like fate and reveals a facultative proliferative capacity in aged beta-cells. Development. 142:3637–3648.

Pauklin S, Vallier L. 2013. The cell-cycle state of stem cells determines cell fate propensity. Cell. 155:135–147.

Prokunina-Olsson L, Welch C, Hansson O, Adhikari N, Scott LJ, *et al.* 2009. Tissue-specific alternative splicing of TCF7L2. Hum Mol Genet. 18:3795–3804. doi: 10.1093/hmg/ddp321. Epub 2009 Jul 14. PMID: 19602480; PMCID: PMC2748888.

Robinson JT, Thorvaldsdottir H, Winckler W, Guttman M, Lander ES, *et al.* 2011. Integrative genomics viewer. Nat Biotechnol. 29:24–26.

Romer AI, Singer RA, Sui L, Egli D, Sussel L. 2019. Murine perinatal beta-cell proliferation and the differentiation of human stem cell-derived insulin-expressing cells require *Neurod*1. Diabetes. 68:2259–2271.

Sadoul K, Lang J, Montecucco C, Weller U, Regazzi R, *et al.* 1995. SNAP-25 is expressed in islets of Langerhans and is involved in insulin release. J Cell Biol. 128:1019–1028.

Sander M, Neubuser A, Kalamaras J, Ee HC, Martin GR, *et al.* 1997. Genetic analysis reveals that *Pax6* is required for normal transcription of pancreatic hormone genes and islet development. Genes Dev. 11:1662–1673.

Schneider CA, Rasband WS, Eliceiri KW. 2012. NIH Image to ImageJ: 25 years of image analysis. Nat Methods. 9:671–675.

Schwitzgebel VM, Scheel DW, Conners JR, Kalamaras J, Lee JE, Anderson DJ, *et al.* 2000. Expression of *Neurogenin3* reveals an islet cell precursor population in the pancreas. Development. 127: 3533–3542.

Sever D, Hershko-Moshe A, Srivastava R, Eldor R, Hibsher D, *et al.* 2021. *NF-kappaB* activity during pancreas development regulates adult beta-cell mass by modulating neonatal beta-cell proliferation and apoptosis. Cell Death Discov. 7:2.

Sharon N, Vanderhooft J, Straubhaar J, Mueller J, Chawla R, *et al.* 2019. Wnt signaling separates the progenitor and endocrine compartments during pancreas development. Cell Rep. 27:2281–2291.e5.

Singer RA, Arnes L, Cui Y, Wang J, Gao Y, *et al.* 2019. The long noncoding RNA paupar modulates *Pax6* regulatory activities to promote alpha cell development and function. Cell Metab. 30:1091–1106.e8.

Soufi A, Dalton S. 2016. Cycling through developmental decisions: how cell cycle dynamics control pluripotency, differentiation and reprogramming. Development. 143:4301–4311.

St-Onge L, Sosa-Pineda B, Chowdhury K, Mansouri A, Gruss P. 1997. *Pax6* is required for differentiation of glucagon-producing alpha--cells in mouse pancreas. Nature. 387:406–409.

Sun Y, Dykes IM, Liang X, Eng SR, Evans SM, *et al.* 2008. A central role for *Islet1* in sensory neuron development linking sensory and spinal gene regulatory programs. Nat Neurosci. 11:1283–1293.

Sund NJ, Vatamaniuk MZ, Casey M, Ang SL, Magnuson MA, Stoffers DA, *et al.* 2001. Tissue-specific deletion of *Foxa2* in pancreatic beta cells results in hyperinsulinemic hypoglycemia. Genes Dev. 15: 1706–1715.

Swisa A, Avrahami D, Eden N, Zhang J, Feleke E, *et al.* 2017. *Pax6* maintains beta cell identity by repressing genes of alternative Islet cell types. J Clin Invest. 127:230–243.

Tao W, Zhang Y, Ma L, Deng C, Duan H, *et al.* 2018. Haploinsufficiency of *Insm1* impairs postnatal baseline beta-cell mass. Diabetes. 67:2615–2625.

Wang H, Gauthier BR, Hagenfeldt-Johansson KA, Iezzi M, Wollheim CB. 2002. *Foxa2* (*HNF3beta*) controls multiple genes implicated in metabolism-secretion coupling of glucose-induced insulin release. J Biol Chem. 277:17564–17570.

Wang S, Yan J, Anderson DA, Xu Y, Kanal MC, *et al.* 2010. *Neurog3* gene dosage regulates allocation of endocrine and exocrine cell fates in the developing mouse pancreas. Dev Biol. 339:26–37.

Wickramasinghe VO, Venkitaraman AR. 2016. RNA processing and genome stability: Cause and consequence. Mol Cell. 61:496–505.

Zhang Z, Xu L, Xu X. 2021. The role of transcription factor 7-like 2 in metabolic disorders. Obes Rev. 22:e13166. doi: 10.1111/obr.13166. Epub 2020 Dec 4. PMID: 33615650.

Communicating editor: B. Andrews